A branching, positive relief network in the middle member of the Medusae Fossae Formation, Equatorial Mars - evidence for sapping?

Journal Item

www.elsevier.com/locate/pss

A branching, positive relief network in the middle member of the Medusae Fossae Formation, Equatorial Mars - evidence for sapping?

S.K. Harrison, M.R. Balme, A. Hagermann, J.B. Murray, J.-P. Muller, A. Wilson

PII: S0032-0633(13)00145-1
DOI: http://dx.doi.org/10.1016/j.pss.2013.06.004
Reference: PSS3541

To appear in: *Planetary and Space Science*

Received date: 5 November 2012
Revised date: 28 May 2013
Accepted date: 10 June 2013

Cite this article as: S.K. Harrison, M.R. Balme, A. Hagermann, J.B. Murray, J.-P. Muller, A. Wilson, A branching, positive relief network in the middle member of the Medusae Fossae Formation, Equatorial Mars - evidence for sapping?, *Planetary and Space Science,* http://dx.doi.org/10.1016/j.pss.2013.06.004

A branching, positive relief network in the middle member of the Medusae Fossae Formation, Equatorial Mars – evidence for sapping?

S. K. Harrison[1*], M. R. Balme[2,3], A. Hagermann[2], J. B. Murray[4], J-P. Muller[5] and A. Wilson[2]

[1]Laboratoire de Géologie de Lyon, Université Claude Bernard Lyon 1 / ENS Lyon, 69622 Villeurbanne Cedex, France.
[2]Department of Physical Science, The Open University, Walton Hall, Milton Keynes, MK7 6AA, UK
[3]Planetary Science Institute, 1700 East Fort Lowell, Suite 106, Tucson, AZ 85719, USA
[4]Environment, Earth and Ecosystems, The Open University, Walton Hall, Milton Keynes, MK7 6AA, UK
[5]University College London, Department of Space & Climate Physics, Mullard Space Science Laboratory, Holmbury St. Mary, Dorking, RH5 6NT, UK

*Corresponding author, samantha.harrison@univ-lyon1.fr

Pages: 54 (including figure captions)

Tables: 2

Figures: 32

Proposed Running Head: A positive relief network in the middle member of the Medusae Fossae Formation

Correspondance to:

Samantha K. Harrison
[1]Laboratoire de Géologie de Lyon,
Université Claude Bernard Lyon 1 / ENS Lyon,
69622 Villeurbanne Cedex,
France.

Email: samantha.harrison@univ-lyon1.fr

ABSTRACT

The Medusae Fossae Formation (MFF) is a geological formation comprising three geological units (members) spread across five principal lobes. It dominates a quarter of the longitudinal extent of the equatorial region of Mars. Positive relief features referred to as 'sinuous ridges' (commonly interpreted as inverted paleoflow channel or valley fills) have been observed in the lowest member of the western MFF, but have not been identified within the central and eastern portions of the formation, in the middle and upper members. This paper presents the identification and analysis of a branching, positive relief system which occurs in the central lobe of the MFF in what appears to be an exposure of the middle member. A simple geomorphological map of the system is presented, from which we have adopted the working hypothesis that this is an inverted fill of a branching fluvial channel or valley system. A suite of morphological and topographic evidence supporting this hypothesis is presented, including analysis of the network using a ~ 15 m per pixel digital terrain model derived from a Context Imager (CTX) stereo image pair. The evidence supporting this hypothesis includes: 1) The local slope and topography of the upper surface of the network are consistent with a contributory network, 2) The braided, fan-like form at the termination of the branching network is consistent in morphology with it being a depositional fan at the end of a fluvial system, 3) The terminal fan and surrounding deposits show layering and polygonization, 4) There is strong association between the lower order branches and amphitheater shaped scarps in the depression walls. We evaluate the possible origins of this fluvial system and suggest that seepage sapping is the most probable. Two possible models for the evolution of the network and related features are presented; both require melt of ice within the MFF to form liquid water. We conclude that at least some portions of the Medusae Fossae Formation, if not the entire formation, were once

volatile-rich. Finally, we note that our observations do not rule out the case that this network formed before MFF emplacement, and has since been exhumed. However, this conclusion would suggest that much of the surrounding terrain, currently mapped as middle-member MFF, is not in fact MFF material at all.

1. Introduction

This work details the mapping and analysis of an unusual set of martian geomorphological features (Fig. 1) located on the central lobe of the Medusae Fossae Formation (MFF), centered at roughly 5°S, 179°E. These features include a branching linear positive relief system located within a scallop-edged depression and an associated large crater. The whole assemblage occurs within terrain mapped as MFF material. The MFF is a geological formation comprising three geological units (members) (Greeley and Guest, 1987; Scott and Tanaka, 1986) spread across five principal lobes (for the purposes of this work labeled A, B, C, D, E). The MFF dominates roughly a quarter of the longitudinal extent of the equatorial region of Mars (Fig. 2), extending east-west across a distance of ~ 5,500 km between the southern Elysium Planitia and the Tharsis region (130-240 E, 15 N-15 S (Bradley et al., 2002; Scott and Tanaka, 1986; Tanaka, 2000). The positive relief feature is the principal interest in this work, as numerous similar examples (referred to as sinuous ridges, or 'SRs'; (Burr et al., 2009; Burr et al., 2010) have been observed over the two westernmost exposures of the MFF, in the formation's lowest geological member, but have yet to be mapped any further eastward or in the middle and upper members (Burr et al., 2009; Burr et al., 2010; Zimbelman and Griffin, 2010). The presence of such a feature in the central lobe, within an apparent exposure of the middle member, may have important implications regarding the volatile content of the MFF.

1.1 Medusae Fossae Formation: Regional context, morphology and origin

Overlying both the older Southern highlands and the younger Northern lowlands, the MFF deposits cover a north-south extent of many hundreds of kilometers and, in some places, up to a thousand kilometers (Tanaka, 2000). Bradley et al., (2002) estimated the areal extent of the current MFF as being 2.2×10^6 km and the palaeo-extent up to 5×10^6 km^2. However, Harrison et al. (2010) suggest this may be an underestimation of the palaeo-extent, as they identified outliers of MFF on the cratered highlands south of the main lobes. The location and stratigraphic position of the MFF, mantling the crustal dichotomy boundary and the transition between the lowlands and highlands, is particularly important, given both the unusual and enigmatic nature of the MFF deposits themselves and the boundary itself: to date no clear consensus has been reached as to the origin of either.

The MFF is typified by a surface with a discontinuous, highly eroded appearance at kilometer to meter scales. It occurs in five primary outcrops or lobes which have been further mapped into three separate geological members: lower, middle and upper (Greeley and Guest, 1987; Scott and Tanaka, 1986). As a whole, the morphologic criteria for identification of MFF materials, as reviewed by Harrison et al. (2010), are: 1) discontinuous nature; 2) the presence of yardangs, either individually or in fields; unidirectional and bidirectional; 3) other erosional and aeolian modification features; 4) the presence of ripple and ridge features; unidirectional and bidirectional; and 5) pits and pit chains, often progressing into mesa formation.

It is commonly agreed that the materials that compose the formation are fine-grained and friable in nature (Edgett et al., 1997; Parker, 1991; Zimbelman et al., 1996; Zimbelman et al., 1997). This long-standing interpretation is rooted in the observed prevalent modification of its

surface by aeolian erosion. For example, the most prominent surficial features of the MFF are tapered ridges called yardangs, an aeolian feature that occur primarily in areas of easily erodible materials (de Silva et al., 2010; Goudie, 2007; Greeley and Iverson, 1985, p. 135). Yardangs have been found to occur ubiquitously over the formation, often in large clusters or fields, as is typical for these features on Earth (Breed et al., 1997; Greeley and Iverson, 1985, p. 135). Some studies have also investigated the progressional development of yardangs, linking them with other surface features including mesas and troughs (Mandt et al., 2008)

Current interpretation, based upon relative stratigraphy and crater counts, places the MFF as a geologically young unit of Amazonian age. However, recent work by Kerber and Head (2009, 2010) and Zimbelman and Scheidt (2012) supports earlier suggestions (Head, 2001; Head and Kreslavsky, 2004) that initial emplacement may have been as early as the Hesperian. This has been based on layering characteristics within the formation, which indicate deposition was likely to be periodic, and mold/cast features (Kerber and Head, 2010), which suggest the formation predates young deposits of the Cerberus plains. Importantly, the origins of the MFF remain uncertain, despite numerous studies aiming to better constrain the age, distribution and material properties. Such studies have resulted in varied hypotheses being proposed to account for the MFF's existence, including volcanic deposits (Scott and Tanaka, 1982), palaeo-polar deposits (Head and Kreslavsky, 2001; Schultz and Lutz, 1988) and lacustrine/oceanic origins (Parker, 1991, 1994).

Over time, some of these hypotheses have been discounted based on the available evidence (for a more in-depth overview of the origin theories see Mandt et al., 2008). Dielectric properties derived from recent radar studies (Carter et al., 2009; Watters et al., 2007a) in particular have

indicated that materials are probably either dry, low density deposits (for example volcanic ash) or ice-rich particulate deposits (Carter et al., 2009; Keszthelyi and Jaeger, 2008; Watters et al., 2007a). Note that although the RADAR data are consistent with ice-rich particulate deposits, they do not provide direct evidence that ice is or was present within the MFF. The possibility that the MFF is ice-rich is just one of at least two working hypotheses, and the available radar data are not able to discriminate between ice-rich or ice-poor conditions.

1.2 Sinuous positive relief landforms in the Medusae Fossae Formation

Positive relief channels are a well-studied phenomenon on Earth and can form when a fluvial channel fill becomes more resistant to erosion than the terrain around it, remaining high-standing as erosion occurs (Pain and Ollier, 1995a). Numerous sinuous and branching positive relief landforms have been observed globally across Mars and, based on their morphology, are often interpreted to be relict, inverted channel fills (Burr et al., 2009; Williams et al., 2009; Williams et al., 2011). Williams et al. (2009) note that the diverse range of morphologies observed amongst such features speaks of a range of palaeo-environments and thus a complex martian fluvial history. Those positive relief channel fills specific to the MFF region were first noted and then surveyed on the regional scale by Burr et al. (2009) and characterized under the term sinuous ridges (SRs; Burr et al,, 2010. In those works, it was found that these features occur exclusively on and around the westernmost lobes of the MFF. The large population of >150 SRs observed across the western MFF has been used to derive a classification scheme, based upon individual SR morphologies and the network forms associated with them (Table 1; after Burr et al, 2009). Zimbelman and Griffin (2010) later refined this scheme on the basis of further observations (Table 2). The majority of these SRs have been interpreted as fluvial in origin but there is less agreement on the source of the fluid involved. Zimbelman and Griffin (2010)

propose that the combined characteristics of most are more consistent with open channel flow and not sub-glacial (esker) flow, although Williams et al. (2009) note that some SRs do appear to be more consistent with the latter interpretation. Further work by Burr et al. (2010), which included paleodischarge calculations, further supports this conclusion: they suggest that over 80% are interpretable as some aspect of fluvial channel fill. Most recently, LeFort et al. 2012 suggested a fluvial origin for all the MFF SRs. The most commonly suggested processes for origin are impact released volatiles, precipitation, or glacio-fluvial flow (Burr et al, 2009; 2010; Williams et al., 2009). For the majority of MFF SRs, no evidence has been found for a tectonic or aeolian origin. However, Burr et al. (2009) identified at least one example which they suggest is a perched volcanic lava flow.

The inversion of valley relief subsequent to fluvial infilling activity can be associated with a number of different induration processes, such as armoring of channel floor by coarser grains, infilling by more resistant materials or even capping by lava flows that followed the valley path (Burr et al., 2010; Hardgrove et al., 2010; Pain and Ollier, 1995b; Zimbelman and Griffin, 2010). Additionally, cementation of the channel fill in the form of, for example, carbonates, sulfates, iron oxides and silicate clays is well documented for terrestrial inverted channel fills (Pain et al., 2007; Williams et al., 2009). The cementation process is considered by Burr et al. (2010) to be the most likely inversion mechanism for the MFF SRs, particularly as it is perhaps the best method to preserve existing sedimentary structures, such as layering, which are seen in some martian examples.

With regard to stratigraphic occurrence within the MFF, SRs have been observed at both multiple and distinct levels (Burr et al., 2009), although the lack of examples over the central to eastern areas of the MFF suggests that they may occur only in and around the lower member (the

lower member only crops out in the western/central MFF, lobes A, B, C; Burr et al, 2009; Zimbelman and Griffin, 2010). Here, though, we describe an isolated and unusually complex SR feature in the central outcrop of the formation that appears instead to be in the middle member of the MFF.

1.3 Study area context: the central outcrop of the Medusae Fossae Formation

The middle outcrop (lobe C; Fig. 2) of the MFF is centered at ~ 5°S, 181°E. It is the largest of the five lobes, and the only one to have exposures of all three members (Scheidt and Zimbelman, 2011). The set of landforms described here occurs in an exposure mapped as the middle member of the MFF (Scheidt and Zimbelman, 2011b; Scott and Tanaka, 1986), in the central portion of lobe C, centered at ~5°S, 179°E (Fig. 3). The specific region of interest occurs in materials typified by an extremely degraded appearance (Fig. 4).

2. Geomorphological observations and interpretation of the study area

All observations of the study area were carried out using imaging data from the High Resolution Imaging Science Experiment (HiRISE; McEwen et al., 2007) at ~ 30 cm/pixel resolution or the Context Imager at ~ 6 m/pixel (CTX; Malin et al., 2007). Both these instruments are on the Mars Reconnaissance Orbiter spacecraft. These data were processed using USGS ISIS software and imported into a GIS for analysis.

2.1 General observations

The study area consists of a scalloped-edged depression of ~ 16 km diameter, which itself intersects with a large, almost circular crater to the north that is ~ 20 km in diameter (Fig. 1). The northern crater is roughly 600 m deep, and the southern depression is just under 400 m deep (all depths from CTX derived DTM, see section 2.7.1). The southern depression contains a branching positive relief feature which is over 14 km in length and over 11 km in width. The southern depression has irregular margins and is bounded mainly by cliffs that, even at 6 m/pixel resolution (i.e. in CTX images), appear very blocky and host many large boulders at the base of the scarp. Talus slopes also occur in a number of areas. At the intersection between the southern depression and the northern crater, material appears to have flowed from south to north across the margin, as demonstrated by a fan-shaped deposit in the southern part of the northern crater. The western half of the northern crater and much of the southern depression floor are both overlain by a deposit which has a lower albedo than the surrounding surfaces in both HiRISE and CTX images. A simple geomorphological map of the area is presented in Fig. 5. The topography of the upper surface of the network shows a general downhill trend in the south to north direction.

The overall first impression of this system is that it is an inverted fill of a branching channel system originating in the southern depression and debouching into the northern crater. We use this as our working hypothesis to provide a framework for understanding the origin of this system, and in the next part of this paper describe the morphological evidence that can be used to test this hypothesis. We also consider a second hypothesis, that seems to us the only other plausible way such a feature could have formed: that this is an erosional remnant created by downwearing and backwearing as material within the MFF was removed.

2.2 Surface and structural characteristics of the positive relief feature

2.2.1 Overview

The branching positive relief feature has large (often near right-angled) junction angles between the branches. The margins of the positive relief feature are uneven, rather than smoothly paralleling the general trend of the ridge. If this feature is an inverted channel fill system, the branching pattern could be described as contributory – starting from several discrete sources which converge into a main channel – or distributary – starting from one main source and splitting into smaller branches (Ritter et al., 2002, p. 391). Given the presence of a fan-like feature at the breach of the northern crater, and the general topographic trend as derived from the global MOLA DEM (MOLA Science Team, MSS/ JPL/NASA.), we suggest the system is contributory. Using Strahler's stream ordering system (Strahler, 1952), it can be described as having up to fourth order branches. The smallest first and second order branches have a simple ridge-like appearance, are relatively narrow (~ 100 to 200 m wide) and often degraded in appearance. In contrast, the larger third and fourth order branches have relatively flat upper surfaces and are up to a kilometer or so across. The main 'trunk' is 3 km at its widest point where it changes into a broad, flat area which directly abuts the margin between the enclosing depression and the larger crater to the north. The enclosed setting of this system is particularly striking. Such a setting is unique within the MFF, as no other example as yet observed in the western materials has been fully enclosed in this manner.

At the regional scale there is nothing apparent in the regional planform observations that is strikingly inconsistent with the working hypothesis that this is an inverted channel fill system. Of note, though, are the high intersection angles of the network, and the broadness of the higher

order branches compared to the small size of the network, both of which seem unusual in terms of terrestrial fluvial networks.

2.2.2 Upper surfaces of the inverted network feature

At 6m/pixel CTX resolution, the top surfaces of the trunk and third/fourth order branches range in texture and can appear smooth at ~ 6 m resolution or minimally modified in some areas (Fig. 6). However, examination at HiRISE resolution reveals even the smoothest areas are actually significantly modified surfaces, typified by extensive surface cracking and containing small impact craters. Scattered mounds and mesa-like projections with smooth edges are also common on the surface of the inverted feature and it is difficult to determine, even at HiRISE resolution, whether these surface projections are a degraded superposing unit, integral to the inverted feature itself, or are a manifestation of underlying terrain.

Linear cracking occurs over most of the top surface of the network and is almost always parallel to the long direction of the inverted feature (Fig. 7). It is particularly well defined at the branching junctions. The cracks range in width from those at the limit of HIRISE image resolution (~ 30 cm) to those several meters across. The cracks are commonly parallel or sub-parallel to each other and there is some minor horizontal cracking, which creates a polygonization effect in some areas.

Due to their linear nature and orientation, we interpret these cracks to be fractures caused either by the relaxation of the materials, following the removal of overlying material, resulting in cambering, or lateral slumping due to the removal of lateral supporting material during preferential erosion of the surroundings. These observations are consistent with the interpretation of an inverted channel fill system in which channel fill material remained upstanding as

supporting material was removed from around it by differential erosion. However, the interpretation of the cause of the cracking is also consistent with the alternate, erosional formation hypothesis.

2.2.3 Branch morphology

The edges of the inverted feature have a jagged appearance. The first and second order branches often appear to be straightforwardly ridge-like at regional scale, however their meter-scale morphology is much more complex. In some cases, the branches appear assymetrical in cross section, with a gentle slope on one side and a steeper cliff face on the other (Fig. 8a), and they can also appear flattened at their ends and barely appear to rise above the depression floor (Fig. 8b). Additionally, in several examples, the first order branches originate either very close to the southern depression edge or actually appear to stem from it. A further point of interest is the occurrence of smaller inverted ridges on top of a portion of a first order branch (Fig. 9) It is possible that they represent a multi-level inversion scenario, as has been discussed for 'multi-level SRs' in other regions (Burr et al., 2009).

The margins of the ridge system are not typified by simple steep scarps: at HiRISE resolution, it can be seen that the majority of the network, particularly the widest, flattest branches, 'step' downwards at their margins (Fig. 10). We infer that horizontal or sub-horizontal layering or planes of weakness are/were present within the ridge, which show themselves as steps when they were exploited by differential erosion. The stepping may be indicative of a compositional or mechanical layering, or it may also represent internal faulting or fracturing. Whist neither scenario is entirely inconsistent with our working hypothesis, the former is more likely to indicate multiple, distinct fluvial episodes within the system, or periods of different flow

strength (and hence different sedimentation characteristics) during one fluvial event. Layering or planes of horizontal weakness are not inconsistent with an erosional origin for the ridge network, but we note that multiple layers are not seen to crop out at the margins of the southern depression, nor in the northern crater walls, as might be expected if this were an erosional landform within terrain of horizontal, "layer-cake" stratigraphy.

2.3 Southern depression

The depression in which the dendritic inverted form sits has deeply scalloped margins, which generally take the form of steep cliffs, except in the south where the slope of the margin is significantly shallower than anywhere else. The blocky and highly modified nature of the depression margin is clearly visible at HiRISE resolution. It is also apparent that the cliff consists of two layers and that there is an obvious contact between these two, wherein a thinner, comparatively dark layer overlies a thicker light-toned layer (Fig. 12). The talus and boulder debris visible at the base of the cliffs are consistent with mass wasting caused by the overlying layer being undercut. The scalloped niches in the depression edge correspond strongly with the origin of first order streams and from this observation we infer that these niches are genetically related to the ridge network (Fig. 11). Such an interpretation is consistent with the fluvial working hypothesis, but there appears to be no reason why this would be the case if the ridge network was formed by erosion. Hence this observation does not support the alternate hypothesis.

The correspondence between the lower order branches of the inverted network and the amphitheatre shaped scarps in the depression wall suggest that, if this network is indeed an

inverted fill of a fluvial channel system, then headward erosion into the depression wall was probably caused by fluvial flow across, or from out of, the depression margin.

2.4 Morphology and textures of northern crater and its floor

2.4.1 General characteristics

In contrast to the depression to the south, the walls of the northern crater have shallow slopes around the entire circumference and the floor appears relatively flat, rather than concave, which we interpret to mean that the crater has been infilled.

2.4.2 Overlying low albedo unit

Approximately half the crater floor is obscured by a deposit of low albedo materials, which covers ~ 144 km^2 and reaches almost to the top of the western crater rim. Morphologically similar deposits cover small portions of the north-western part of the southern depression floor between the branches of the inverted network. Similar deposits are also visible on lobe C (Fig. 13), near the contact between the middle and upper members, ~ 50 km south of the study area described here. These dark materials appear to be the youngest in the study area, infilling topographic lows and overlying all other features, and contain few, if any, impact craters. The marginal regions of these deposits, especially in the north and southwest of the northern crater (Fig. 14) are morphological similar to small aeolian features known as Transverse Aeolian Ridges, or TARs (Balme et al., 2008; Berman et al., 2011; Bourke et al., 2003). However, the bulk of the dark deposits do not appear similar to either TARs or the larger dark dunes that typify aeolian bedforms on Mars (Cutts and Smith, 1973), so it is unknown whether the entire deposit is aeolian in origin, or if instead the marginal TAR-like forms are reworked aeolian landforms

caused by degradation of the dark material. We conclude that the dark materials are a geologically recent lag, mantle or mass-wasting deposit, of possible, but not definitive, aeolian origin.

2.4.3 Possible depositional textures

The material which covers the remainder of the northern crater floor appears to be of a similar origin to the branching inverted feature to the south. There are several pieces of evidence to suggest this. 1) The crater floor material is similar in appearance and surface roughness to the tops of the inverted network to the south. 2) Material appears to have been transported through a "breach" between the southern depression and the northern crater. Following the working hypothesis we infer that the southern inverted network was the conduit for this material and the fan-like deposit beneath the breach, and the floor of the northern crater, represent depositional zones of this transport system. Directly north of the breach is a region showing what appears to be a complex system of small, (perhaps braided) positive relief features; Fig. 15). This region extends to about 7 km from the breach. The surface morphology and fan-like form are similar to regions of a fluvial system where both transport and depositional processes occurred. This braided, fan-like form is similar in morphology to terrestrial alluvial fans, which often occur where a change in topography results in unconfined flow. Such fans on Earth are commonly triangular in planform shape (Easterbrook, 1999, p.159), much like this example. None of the observations of this fan-like feature or the crater floor appear to be consistent with an erosion-only formation hypothesis for the positive relief ridge network.

2.4.4 Other crater floor textures

In the eastern part of the crater floor there is an area roughly 2.5 km across that appears uneven and rough in CTX images. Closer examination in HiRISE shows that this is caused by distinct layers that have been eroded to form curved and lobate patterns, resulting in numerous mesa type features with clearly stepped edges (Fig. 16). We suggest the most plausible interpretation is that this terrain represents stacks of horizontal layers, such as would be deposited in a lake environment, that have undergone significant differential erosion. In the north-eastern portion of the crater, the HiRISE coverage ends at the southern extent of a region typified by a distinctive pattern of albedo 'swirls' in the CTX images (Fig. 17). The easternmost of the adjacent HiRISE image covers a small portion of this region, and the finer resolution reveals that this pattern is very similar to the rough textures shown in Fig. 16. We infer that this texture is also caused by differential erosion of stacks of layered terrains; what would be clearly seen as layering in a HiRISE image instead results in the 'swirl' appearance in CTX images.

Over several areas of the crater floor, polygonal patterns (a few meters across; Fig. 18) of surface cracking can be observed. Such textures can be indicative of former ice-content, with similar features, thought to have formed by thermal contraction cracking of ice-rich sediments, being widespread across the martian mid- to high-latitudes (Mangold, 2005) and rarely at low latitudes (Balme and Gallagher, 2009). Polygonal patterned grounds on Mars have also been interpreted as desiccation cracking (El Maary et al., 2010; Seibert and Kargel, 2001), and cooling cracks in lavas (Keszthelyi et al., 2004). They could also be jointing fractures. Given the geological setting, it is unlikely that these surfaces terrains are volcanic in origin. Instead, the patterns of erosion and polygonization are consistent with episodic fluvial deposits. In this scenario, the polygonization could represent desiccation cracking or thermal contraction cracking

in ice-rich sediments. Once again, such observations are consistent with the fluvial working hypothesis but are either inconsistent with, or unrelated to, testing the erosional hypothesis.

2.5 Medusae Fossae materials

The exposure of the middle member in which this feature set occurs is not typified by the presence of distinctive, highly defined MFF yardangs. However, yardangs do appear over significant areas of the southern depression floor. There is a variety of outcrop sizes, and in many cases yardangs occur between the branches of the inverted network, often abutting against them. Indeed, in some areas, it seems that the MFF yardangs appear to have been eroded out from the edge of the inverted feature itself (Fig. 19), although this interpretation is uncertain, even when made by examination of HiRISE images. Small individual yardangs, sometimes clustered closely together, also occur on the top surfaces of the flattest branches (Fig. 20). These seem to have formed from a discrete layer on top of the inverted network, rather than having eroded from it, suggesting that the network itself was buried at some point after formation. We interpret these as yardangs, rather than dunes, due to their classic 'ship's hull' appearance, with one blunted end. There are no MFF materials visible on the floor of the crater, in contrast to other craters in the region in which MFF materials are clearly visible. There is also no evidence of yardangs eroding out from the resurfacing material that fills the northern crater. This suggests that the crater floor has been substantially infilled by debris and deposits from the southern branching system. If the branching network sits within the MFF, then these debris and terminal deposit materials have effectively armored the underlying MFF material in the same way as occurred in the branching network system that now has positive relief, reinforcing the idea that both the network and the distal debris materials are significantly more resistant to erosion than the MFF. Furthermore, the

observations of a few yardangs on top of the branching network could imply a later stage of MFF deposition and erosion. An alternative which must be considered is that the branching network, and the topography in which it sits (i.e. the southern depression and the northern crater), both formed underneath, or prior to the emplacement, of the MFF. This idea is discussed in section 3.4.

2.6 Impact cratering

There only 21 recognizable impact craters with diameter above 15 m on the branching inverted system itself. The largest impact craters are on the main branch and the other flat inner branches are ~ 125 m in diameter. This could indicate either that this is a relatively young surface or that it has only relatively recently been exhumed. Most of these craters appear to postdate the surface cracking described in 2.2.2.

The floor of the northern crater is also lightly cratered, with the largest example being ~1.5 km in diameter, and which is partially buried by the dune deposits in the west. Several smaller craters also appear to be infilled with the same material. No craters can be seen on the aeolian deposits themselves, indicating that they are relatively young. Additionally, there is at least one example in the west of the northern crater of an apparently inverted crater ~ 70 m in diameter with stepped edges (Fig. 21). This suggests an induration process within the crater, followed by erosion, in a similar way to that which created the 'swirl' albedo patterns in the northern crater and the positive relief of the branching network in the south.

The 'swirl' patterned region of the crater floor hosts at least six examples of raised ejecta craters (Fig. 22a). These range in size both in terms of the crater diameters (20 m to 60 m) and in the diameters of their ejecta blankets (150 m to 600 m at the widest point). The ejecta are

consistently asymmetrically lobate with the greatest part of the ejecta spread predominantly to the northeast and southwest. Of particular interest is the fact that a raised ejecta crater , ~ 60 m in diameter, on the surface of the inverted network to the south, shares matching asymmetry, with the ejecta extending up to 280 m outward from the central point. Such asymmetrical 'butterfly' shaped ejecta patterns have been associated with clusters of secondary impacts – with the consistently asymmetrical shape of the ejecta being a function of the direction of the primary impact (Calef et al., 2009; McEwen et al., 2005).

All these craters have the same asymmetric axis to their ejecta, and are for the most part clustered together, which suggests they were formed at the same time, perhaps as secondary craters from a larger impact (Calef et al., 2009; McEwen et al., 2005). That these examples of raised ejecta craters with consistent asymmetrical ejecta patterns have been observed on both the northern crater floor and the southern inverted network might serve as a temporal stratigraphic reference and hence could indicate that these regions were both subaerial (exposed) at the time of impacts.

2.7 Topographic and quantitative analysis

Thus far, we have presented the qualitative evidence from planview imaging data. Next, we discuss such quantitative topographic data that exist.

2.7.1 Digital terrain model for the study area

The most reliable topographic data available are the MOLA point and the interpolated MOLA gridded data (Smith et al., 2000). However, although these data provide precise heights, they are too coarsely spread to allow more details of the shape of the terrain to be obtained. Figure 23 shows the distribution of MOLA points over the study area. The study area has

coverage by both an HRSC stereo pair and a CTX stereo pair, either of which can be used to generate a DEM from stereo images. The appropriate HRSC stereo pair was unfortunately too noisy to be of use, but the CTX stereo pair allowed a ~6m/pixel CTX DTM to be generated using the Ames Stereo Pipeline; Fig. 24). Unfortunately, problems with image registration meant this DTM could only be produced as a relative dataset, not one absolutely tied to the MOLA data or the original images. In comparative profiles, the CTX DTM differed in height from the MOLA DEM by a consistent value of about 860 m. The areas where divergence was greatest were found to correspond to the areas of steepest terrain or errors in the DEM. Outside these regions, the corrected CTX values were usually within 25-50 m of the raw MOLA data points from the same location. This was judged to be an acceptable level of deviation and so the CTX DTM was used to generate the profiles discussed in the following subsections.

2.7.2 Regional profiles

As indicated by the regional slope trend in the MOLA data, the local slope across the branching feature is south to north (Fig 25a). The depression is a maximum of 500-550 m deep, whilst the crater is over 600 m deep at its lowest point. Obviously the depression floor has a variable base level due to the presence of the inverted channel fill, whilst the crater floor is relatively smooth in comparison.

Although the regional slope is approximately horizontal in the east-west direction, the depth of both the crater and depression increases to the east (Fig. 25b). In the case of the crater, this is obviously due to the significant infill on the west side, but may also indicate preferential erosion of the material in the east with deposition in the west. The same process may also then have resulted in an uneven exhumation in the southern depression and might have been a result of a strong prevailing wind direction.

2.7.3 Longitudinal profile of the inverted system

Longitudinal profiles along three largest tributary branches and main trunk of the network (Fig. 26) indicate that there is a general sharp initial drop in elevation, prior to a steadier drop along the majority of the network length, with a total decrease in elevation of just over 200 m. The initial drop is roughly 100 m over a 3 km section. The third branch (to the east) shows a shallower, lower elevation slope and is relatively flat along its length and even appears to trend uphill until it reaches the main trunk. Towards the end of the network, approaching the "breach" between the depression and the crater, the elevation once again drops steeply. For all these profiles, a vertical uncertainty of 25-50m must also be taken into account, based on uncertainty inherent in stereo DTM production (of the order of the pixel size – 6 m) and the apparent disparity with MOLA point values (up to about 50m in the steepest areas, where MOLA point data are more uncertain).

2.7.4 Inverted ridge dimensions

Cross sections of the main branch of the network (Fig.27) can be made from the CTX DEM. The measurements reveal that the cross sectional shape of the positive relief feature changes along its length. The widest sections are also the flattest, whereas the narrow branches almost have an inverted v-shaped. The western side of the main branch is consistently higher than the eastern. The depression itself is deeper on the eastern side, so this asymmetry to the inverted feature could be due to uneven exhumation, infill or regional tilting. The widening of the branching ridge with distance from the depression margin (or distance along channel

following the inverted-channel fill hypothesis) is shown in a plot of width:height ratios against distance downhill (Fig. 28).

2.8 Hypothesis testing

The evidence that is supportive of the fluvial system hypothesis includes:

1) The local slope and topography are consistent with a contributory fluvial network

2) The braided, fan-like form at the termination of the branching network is consistent in morphology with this being a depositional fan at the end of a fluvial system.

3) This depositional region and its immediate surroundings show considerable evidence for layering and polygonisation, consistent with post depositional deformation of sediments laid down in water.

4) There is strong association between the lower order branches and the amphitheater shaped scarps in the depression walls.

In contrast, the purely erosional hypothesis is either inconsistent with the observations, or does not explain them. We therefore suggest that this inverted form was once a fluvial system and that the inverted nature is a result of preservation of the original channel or valley shape due to a greater erosional resistance of the filling material than the surroundings.

As described above, there are several mechanisms by which a fluvial system can become inverted. One previously cited analogue for flat topped inverted channels on Mars are carbonate-cemented fluvial channels in Utah's Green River area (Williams et al., 2009; 2011), and some of these have branching morphologies. However, the presence of carbonates in the MFF materials is unlikely – a carbonate origin for MFF formation has been ruled out (Parker, 1991; Tanaka, 2000; Zimbelman et al., 1996; Zimbelman et al., 1997; Zimbelman et al., 1999). A lava capping

scenario would also seem unlikely, given the lack of possible vents or other volcanic landforms here. A more plausible process by which induration might have occurred is chemical cementation by way of evaporation or sublimation (e.g., Burr et al. 2010). However, there are no diagnostic indicators for any indurating agent on the basis of channel fill form (Williams et al., 2009), making identification difficult for the process by which the channel network became inverted.

3 Discussion

3.1 Channel-depression relationship

When considering the inverted network, the question of how the depression itself originated is also key: was the entire depression there before the network formed, or did the network create or enlarge the depression? The pattern of scalloped niches in this depression shares superficial resemblance to highly modified craters, such as Victoria crater, which was visited by the Mars Exploration Rover 'Opportunity' (Squyres et al., 2009), and also to the amphitheater-type headscarps of groundwater sapping channels such as those described by Irwin et al. (2008) and Bouley et al. (2009). The scalloped and layered appearance of the edges, the occurrence of boulders at the base and the talus on the slopes all indicate failure of the cliff material and relatively active mass wasting processes at the depression edge, but unlike Victoria crater the indented niches in the wall are spatially associated with the smaller, lower order branches, suggestive of a genetic link between the two landforms. Hence, a plausible hypothesis for the scalloped morphology is that this was originally an impact crater, and was expanded by

fluvial processes, perhaps including sapping and/or overland flow across the rim. Arguing against this explanation are the observations that there is no clear topographic indication of a raised rim around the southern depression, whereas one might expect a distinct rim if it were an impact crater. However, the regional deflation associated with the MFF in general could have erased much of the rim topography if it ever existed. If the southern depression was once a simple impact crater then that crater must have been very heavily modified to retain none of the circularity one would expect to see (and contrasting with the crater to the north). If this was a circular impact crater that was later extended to the current margins, the existing relief suggests that such a crater could not have been wider than ~ 11 km, compared to its current diameter of ~ 16 km, as this is the largest circle that can fit into the margins of the depression rim. In this case, post-formation modification would have been biased towards the eastern side of the crater, and could have been genetically associated with the fluvial flow that formed the inverted channel fill and related material. We suggest that removal of the crater rim might have occurred as a result of these processes. We conclude that it is possible that the southern depression could have been created by extension of the initial circular shape by erosional processes which might have included aeolian abrasion or sapping or overland flow. There therefore could have been a depression of some sort in existence before the network was formed, although it was significantly enlarged during, and perhaps due to, the formation of the network. An alternative explanation is that there was initially no depression, and instead this void formed as a result of collapse caused by undermining of the surface by sub-surface fluvial flow. Such a scenario would probably require sapping and significant retrogressive erosion in a southerly direction at the southern margin. This idea is discussed in section 3.7.

3.2 Crater-depression relationship

It is clear from its highly degraded rim, degree of infill and shallow slopes that the northern crater is of significant age and predates the inverted branching network. However it is unclear whether this crater postdates the depression to the south. The intersection between the two is too eroded to be sure of where the original margin may have lain and the regional deflation that has occurred throughout the MFF makes it difficult to infer stratigraphy based on superposition relations between the faintly visible ejecta blanket of the northern crater and the southern depression. This is coupled with another intriguing feature: that the rims of the north and south craters lie almost tangential to each other. There is often a structural instability at the point where such craters intersect, and this can intensify mass wasting even in totally dry environments such as the moon (Guest and Murray, 1969), therefore presenting a weak spot for further (perhaps fluvial) erosion.

3.3. "Swirl deposits" in the northern crater.

There are surface textural similarities between the materials comprising the inverted channel fill system and those that occur across the northern crater floor. The differential erosion on the edges of the channel fill in the south also corresponds to the significant differential incision into the deposits of the northern crater floor, as indicated by the layered and mesa-like textures that form the 'swirl' terrain. Given the spatial extent of the continuous horizontal layering and the polygonal patterns within the swirl-textured material, together with the proximal fluvial fan, an interpretation of these deposits as lake or playa sediments seems reasonable, although not demonstrable with the data available.

3.4 Does this system occur entirely beneath the MFF?

One of the most important issues in determining the stratigraphic position of the network in the regional geology is whether or not the topography in which the branching network occurs predates the MFF or formed within/on top of MFF material. Several strands of evidence have a bearing on this question. Firstly, the apparent genetic link between the shape of the branching network and the scalloped niches in the southern depression rim suggests that the currently visible topography was shaped partly by the formation of the inverted network, and so the materials forming the walls of the depression and crater must have been in place before the network formed. It should be noted also that the southern depression sits within the boundaries of the poorly-defined ejecta blanket of the northern crater, hence if the crater can be shown to have formed before the MFF then the branching network could also have formed before MFF was deposited. However, if the crater formed within the MFF material, then the ridge network cannot have formed before the onset of deposition of MFF materials.

The ejecta blanket of the northern crater, visible in both MOLA topographic data and CTX imaging data, forms a local high point within this lobe of the MFF (Fig. 29). The profile shown in Fig. 29 reveals that the lowest point in the crater is about 2000m below datum and that it occurs within material mapped as middle member (Amm), assuming a horizontal layer-cake style structure. If the crater and depression in which the network occur actually formed before (i.e. are now beneath) the MFF then Fig. 29 suggests that either (i) the MFF members are nothing more than very thin draping mantles, and are not horizontal layers, such that the topography revealed in the profile is indicative of the basement topography, not the erosion and deposition of the MFF or (ii) that the basement terrains beneath the MFF bulge upwards in the area beneath the crater and depression hosting the inverted network feature, and hence that the middle member is very thin here. Neither of these possibilities seems likely, given that the majority of the mapping

work done to date suggests the principal MFF members represent massive deposits of considerable volume (Bradley et al., 2002; Carter et al., 2009; Frey et al., 1998; Mandt et al., 2008; McColley et al., 2005; Scheidt and Zimbelman, 2011a; Shockey et al., 2004; Watters et al., 2007b; Zimbelman, 2010; Zimbelman et al., 1996).

Furthermore, a second strand of evidence comes from the observations that yardangs appear to be being exposed from underneath the branching network (See figures 8, 19). Once again, this is difficult to prove, even given HiRISE images, but if this is the case then this would provide a convincing stratigraphic argument that the branching network formed within and/or on top of surfaces that hosted yardangs (i.e. the MFF).

We conclude that neither the topographic or morphological evidence supports the idea that the network formed before, and hence is now stratigraphically underneath, the MFF. The only way we think this could have occurred is if the middle member unit mapped by Greeley and Guest (1987) and Scott and Tanaka (1986) and shown in Fig. 29 does not represent MFF materials at all, and instead represents materials exhumed from underneath the MFF. We note that there is little morphological evidence for the either the ejecta blanket of the northern crater, or the materials surrounding it, being reworked into yardangs in a "MFF-like" way. If this is the case, not only would this suggest that the branching network is older than the MFF, but it would also suggest that this region of the MFF should not be mapped as MFF material at all. This would necessitate a rethinking of the regional stratigraphy of this lobe and would call into question much of the contact mapping of the middle and lower members in this region. Given the volume of work that has been done here, we do not think this is likely.

We therefore suggest that the topographic and stratigraphic evidence suggest that it is likely that the branching network formed within the MFF, and hence that both the northern crater and the southern depression also formed within the MFF.

3.5 Exhumation

Removal of material and deflation of the terrain have clearly been taking place in this system, as demonstrated by the presence of features similar in morphology to TARs, the mass-wasted cliffs wall of the depression and the exposed layering and mesas. The presence of yardangs on the inverted channel fill near the northern crater provides strong evidence for later burial and exhumation. The fracturing on the channel fill surface, which we interpret to be as the result of removal of supporting material to the sides, could also be indicative of burial and then exhumation.

The apparent uneven exhumation of the fluvial valley fill, wherein the western branches are less defined and the depth of the depression increases from W to E, suggest that these western regions might not be fully exhumed. This in turn suggests preferential erosion and deflation in the eastern portions of the depression. This follows the pattern of the northern crater, in which deposition (or a lack of removal) has been concentrated on the western side. This might reflect regional wind patterns. Observed regional windstreak orientations do suggest a wind direction that would result in preferential material accumulation against the western margins.

3.6 Comparison with SRs in the western MFF

This example of an inverted fluvial valley does not sit well in any of the existing classifications for SRs in the western MFF (Burr et al., 2009; Zimbelman and Griffin, 2010;

Lefort et al, 2012), particularly given its enclosed setting. Nevertheless, if we were to employ Burr et al.'s (2009) and Zimbelman & Griffin's (2010) criteria for sinuous ridge classification, this positive-relief channel fill system most closely fits within the "flat crested ridge category". It has a broad, planar top surface tens of meters across which exhibits little change in elevation across its breadth and has no visible medial ridge in either images or the DTM. However, it could also be classified both as "isolated" and "branched" and is furthermore associated with an impact crater down into which it slopes through a breach in the rim. Zimbelman & Griffin (2010) observed that many flat SRs in the eastern MFF were overlain by a thick layer of MFF materials, which this example does not appear to be. However, it is possible that any such overlying MFF has been almost completely removed by deflation, and there are indeed a few small, remnant yardangs on the surface of the network that appear to confirm burial and subsequent erosion. Interestingly, Burr et al., (2010) interpret a number of flat topped SRs to be meander belts and this seems a reasonable interpretation for the branching network described here.

There is one SR in the westernmost lobe of the MFF that is strikingly similar to the network described here (Figure 30). This example shows a networked SR terminating within a crater at a fan–like deposit, a situation analogous to that observed in our study area. Burr et al., (2009) previously described this SR and classified it as being a branched, multilevel example, associated with a well-developed fan-shape form. They suggested that the occurrence of the fan at the lower end of the SR, together with a decrease in elevation with distance away from the SR, unambiguously supported an interpretation of distributory paleoflow.

3.7 Formation of the positive relief network

The working hypothesis that is consistent with the observations is that the branching network described is an inverted, relict fluvial system. We next consider how such a system might have formed. It has been suggested that for many martian valley networks, a combination of processes including overland flow and groundwater sapping is likely (Carr and Malin, 2000). The source of water for apparent fluvial flows on Mars also remains a contentious issue (Irwin et al., 2008), with possible candidates being release of underground water (i.e. sapping), or precipitation and runoff of liquid water, snow precipitation and melt.

Although perhaps not as straightforward to interpret as "normal" channels, positive relief channel fills can be an excellent indicator of fluvial processes, as they can preserve fluvial sediments and forms in three dimensions (Williams et al., 2009). However, complications can arise when it is not known to what extent the relict inverted network represents the original channel form. It is possible that, for example, a considerable amount of post-incisional widening could have occurred prior to valley infill and subsequent inversion, and that the form represents a broad fluvial system through which only a narrower active channel flowed. Similarly, the fill could represent a channel belt system, or valley floor, rather than an individual channel. In this scenario, it is possible that ridges such as those shown in Fig. 9 represent relict active channel fill and the larger inverted form only the subsequent valley fill. Thus, these factors must be taken in account when assessing possible formation mechanisms for this feature.

Firstly, we consider the source of the water. In terrestrial settings precipitation is a common water source, however, in martian fluvial flow, precipitation is a contentious issue (Carr, 1995; Hynek and Phillips, 2003). Most of the martian valley networks thus far observed have occurred in the oldest Noachian terrain, and were probably emplaced when the climate was warmer and wetter (Carr, 1995; Hynek and Phillips, 2003). Given the geological and latitudinal

context of this feature however – in a material exposure interpreted as relatively young – and the probable past climatic conditions of Mars since this material's deposition (i.e. cold and dry, as may be further supported by meteorite weathering evidence; Wentworth et al., 2005), precipitation of liquid water is not considered an option for the origin of the water. This does not preclude other types of overland flow, for instance catastrophic outflows caused by short term events, which have been considered a likely source of a number of martian valley networks (Carr and Malin, 2000; DeHon and Washington, 2000). Such outflows can be the result of release of volatiles from surface material, for example by impact, volcanic or geothermal processes. Other possible primary sources for martian fluvial flow include those associated with glaciation (for example resulting from glacial melt or sub-glacial flow) or subsurface groundwater (Baker, 2001). Given the unlikeness of precipitation, but the apparent distributed nature of the source, we suggest that the most likely sources for the water are: (i) ice or liquid water within the subsurface (ii) ice or snow at the surface.

Secondly, consider the process by which flow could have occurred. Four possible forms of flow for the formation of this channel system can be proposed: (i) subsurface flow, (ii) sub-glacial flow, (iii) wholly overland flow and (iv) sapping flow (i.e. overland flow forward of sub-surface flow).

(i) Subsurface flow

Although other martian networks have been interpreted to represent channelized subsurface flow similar to that created by solution in terrestrial carbonate rocks (Carr and Malin, 2000), we dismiss this possibility based upon the extreme unlikelihood of the MFF being composed of carbonate materials. Furthermore, the flat and broad

cross-profile of the channels, and the contributory shape of the entire network seem inconsistent with underground flow.

(ii) Sub-glacial flow

Although some MFF SRs have esker-like morphologies, in which inversion occurs through choking of a sub-glacial or englacial flow, followed by removal of the superposing ice, we suggest that the flat and broad morphology of the channel system, as it appears now at least, is inconsistent with an origin as an esker, which tend to be more ridge-like (Menzies and Shilts, 2002), and commonly lack such a number of tributaries. Most importantly, there is no other evidence for glacial activity in the immediate area.

(iii) Overland flow

The main reasons for excluding a purely overland flow hypothesis are the lack of an apparent source, and the absence of similar features in the surrounding area. For example, if this network formed by precipitation-fed overland flow, then similar features might be expected to occur in the surrounding area. Their absence suggests this feature did not form due to regional scale precipitation and runoff. As previously mentioned, overland flow on Mars has often occurred as a result of catastrophic outflow events, as supposed to precipitation (Baker, 2001; Hynek and Phillips, 2003), but there is not an obvious source for such an outflow here. The scale and morphology of the network are also inconsistent with scabland-style events. Amazonian mid-latitude overland flow has been described as a result of thaw of ice within Lyot crater (Dickson et al., 2009), but there is no evidence for glacial-like forms in the southern depression described here, in contrast to Lyot crater.

Alternatively, melting of smaller, transient snow or ice deposited on the depression walls could provide a source of water for overland flow, as has been suggested as a source for the liquid water that carves small gullies (e.g. Levy et al., 2009) but we note that there are no small gullies on the depression walls. Small gullies have been interpreted as overland, hyperconcentrated or debris flow (e.g. Malin and Edgett, 2000), and are common at mid-latitudes on Mars, but are rare this near the equator (Balme et al., 2006; Kneissl et al., 2010). It seems unlikely that the amount of water required to form this network could have been produced by melting of ice or snow packs without leaving a morphological signature on the depression walls. We therefore consider it unlikely that purely overland flow created by melting, precipitation or catastrophic outflow created this feature.

(iv) Sapping

As a formation mechanism for martian valley networks, sapping has been considered one of the likeliest to account for many of their characteristics (Carr, 1995; Goldspiel and Squyres, 2000). The positive relief network shares a number of characteristics with martian features interpreted to be sapping channels, such as those described by Carr (1995), Carr and Malin (2000) and Goldspiel and Squyres (2000). For example, the high angle junctions and amphitheatre headscarps in particular are typical of sapping networks. Additionally, sapping occurs in geological settings where a distinct layer in a cliff occurs as an impermeable layer overlying a more permeable one, and the clear cliff layering described in 2.3 could support such a condition in the depression walls. We therefore consider sapping to be the most likely mechanism.

Although sapping seems a plausible mechanism for the emplacement of this feature, many proposed martian sapping networks have much shorter, stubbier branches and the networks as a whole are more commonly elongate, rather than contained within a circular basin. We present two possible models that could explain this: a) a headward sapping model, and b) a centripetal sapping model.

a) Headward sapping model

Figure 31 shows a cartoon schematic for a development model in which liquid (probably derived from melt of surface or near-surface ice) accumulated in the sub-surface to form a water table which then found an outlet to the surface near the top of the southern rim of the northern impact crater. The flow of liquid caused undermining of material above it, which collapsed into the depression and was carried into the northern crater. As flow continued, further collapse and transport created a backwards-eroding headscarp and formed a sapping valley. Lateral branching of the network could have occurred as flow exploited planes of weakness associated with the impact crater to the north – and indeed many of the approximately E-W trending parts of the network seem to be concentric to the center of the northern crater. The branching relief visible now reflects the subaerial component of this system. Headward erosion would have created and exaggerated the scalloped morphology at the depression edge. This model is consistent with the observation that the regional slope is north to south, at least for 50 km to the south and for much further than this to the north. Hence a local low point created by the crater would have been the natural place for any regional groundwater flow that existed to debouch onto the surface.

The implications of this model are (i) that only the northern crater was in place initially, the southern depression was created as the sapping channel extended south, (ii) an impermeable

layer must have existed within the MFF in this region such that flow occurred on the crater wall, rather than at the foot of the slope, (iii) the circular shape of the southern depression occurred by chance, rather than as a result of there being a pre-existing crater, and (iv) the MFF in this region was ice-rich and of sufficient permeability at a regional scale for groundwater flow to have occurred, following a heating event that melted the ice.

b) Centripetal sapping model

Figure 32 shows a cartoon schematic for a development model in which a centripetal groundwater flow (wherein water flowed inward from recharge areas at the margins of the basin (Todd and Mays, 2005), formed by melt of ice in the subsurface, formed the network. In this model, the liquid exploited pre-existing planes of weakness caused by the northern impact, creating a rectilinear branching pattern. Headward erosion created the scalloped morphology at the depression edge. Expansion of the headward erosion caused the flow to breach the existing crater to the north – perhaps first through groundwater flow. This lowered the base level, essentially redirecting flow northward into the northern crater, resurfacing it and resulting in the anomalously broad terminal trunk section. The dendritic relief visible now reflects the subaerial component. It is difficult to ascertain what local energy source could have driven such melting. One possibility is that a thermal anomaly associated with a relatively small impact formed both the energy source for melt (c.f. the model from Morgan and Head, 2009), and a small originating basin which provided an initial sink and was then enlarged by groundwater flow.

In this scenario, the northern crater was in place before the second smaller impact to the south, which evolved into the depression visible in the present. The implications of this model are (i) that both the northern crater and the southern depression were in place before the network

was formed, (ii) there is no requirement for a regional impermeable layer nor a heat source, as an impact could have created both, and (iii) the MFF in this region was ice-rich and permeable.

The models described above represent our current working hypotheses. We suggest that these models are consistent with more of the observations than other hypotheses involving sub-surface, sub-glacial or purely overland flow. Further hydrological modeling will be required to test if these working hypotheses are plausible.

3.8 Implications for composition of the MFF

Melt of ice in an ice-containing, yet not necessarily ice-rich, MFF is necessary in both the formation scenarios we identified. Such a source of water is consistent with, although not required by, the radar sounding results, as discussed in 1.1, but there is a lack of morphological and geological evidence to support this conclusion in general (Lefort et al., 2012). In this feature set, aside from the flow channels themselves, there are a number of morphologies that could further support (but are not alone diagnostic of) the presence of ice, for example the polygonization on the floor of the northern crater. Polygons near the end of outflow channels may represent ice-rich sediment that underwent post-deposition thermal contraction cracking. Additionally, the raised ejecta craters may indicate impact into a material with a high volatile content since they occur only on those surfaces inferred to be fluvial sediments.

This begs the question as to why the MFF might be volatile rich. There could have been an inherent ice content if the MFF formed as ice-rich dusty deposits including re-worked volcanic fines (Burr et al., 2010), or as cyclical deposits laid down in periods of high obliquity (Head and Kreslavsky, 2004). In relation to the other main working hypothesis for MFF composition – the ignimbrite scenario – Wilson and Head (2009) have presented models in

which layers of pyroclasts more than 2 m in thickness protect existing layers of surface ice. Similarly, Clifford et al. (2010) described a scenario in which martian ground ice could have been buried by the volatile-poor MFF, resulting in vertical redistribution of the ice content and (geologically speaking) rapid charging of the volatile-poor overlying material with ice. Therefore, the MFF, although originally volatile-poor, could have become volatile-rich over time, and perhaps only in certain areas (i.e. those under which there was ice). Burr et al. (2009) suggest an alternative hypothesis, in which the dry, permeable MFF materials are charged with water (and hence ice) from the top down, due to precipitation. They suggest either rainfall or snowmelt might be responsible.

Whether the ice in the MFF was primary or secondary, a significant volatile content and a high permeability substrate provide possible a explanation for the existence of both the western sinuous ridges and the inverted network feature in the central lobe described here, wherein an impact event or geothermal warming triggered a melt of this ice content, resulting in fluvial flow. Furthermore, the high permeability of MFF material would also be conducive to groundwater flow and hence a sapping model (Schmincke, 1998, p. 212). If we assume, in contrast to our models, that the MFF has no ice content, the question of where the water associated with such groundwater flow originated from remains, particularly since the absence of other equivalent features in the middle member suggests this is a unique occurrence.

4. Conclusions

This is an apparently unique inverted network that, unlike other similar SR features, occurs in the western middle member of the MFF and within a closed basin. The scalloped morphology of the southern depression walls appears to be genetically related to the network and

there is a fan-like structure where the highest order branch of the network breaches the northern crater wall. We infer from these observations that this network is a relict, positive-relief, contributory fluvial channel. We suggest that inversion of the network probably occurred as a result of chemical cementation of the channel fill, followed by regional deflation. Channel flow breached the margin of the northern crater, resulting in the resurfacing and infilling of the northern crater floor, and reworking of these deposits has left layered mesas and "swirl" patterns in the northern crater floor, as well as substantial aeolian mantles. Layering in the fluvial deposits may suggest sustained and time-varying, or episodic, fluvial events. It is possible that the northern crater contained a lake.

We do not favor a purely sub-surface or esker-like origin for the network, but instead suggest an origin by sapping, with the subaerial portion of the system becoming indurated and inverted as fluvial activity ceased. Both of the potential sapping models we have considered for the origin and development of these features requires melt of ice to form liquid water within the MFF. This suggests either that the climate must have been conducive to melt at this time or that there was another source of heat such as a local geothermal or impact event. Groundwater flow within the MFF also requires impermeable layers within the MFF, suggesting that there were hiatuses and induration events in deposition of the MFF, possibly consistent with an alternately welded and non-welded zone within a layered sequence of ignimbrite deposits (Mandt et al., 2008).

It cannot be unequivocally demonstrated this system, and the topography it forms in, has not been exhumed entirely from beneath the MFF. We do not think that this is the case, however, based on the morphological and topographic evidence. We note that if this system did form before the MFF was emplaced, this suggests that much of the surrounding terrain is also

exhumed basement, and not MFF at all. This would completely alter the accepted mapping of this region.

Finally, the conclusion drawn for the origin of this networked feature suggests that at least some portions of the Medusae Fossae Formation, perhaps even the entire formation, are, or were, volatile-rich.

Acknowledgements

This work was funded by a UK Science and Technology Facilities Council (STFC) studentship and through the UK Space Agency Aurora Fellowship scheme. The authors would like to thank Dr Pete Grindrod and Zack Moratto for their work generating DTMs, Dr Colman Gallagher for his very helpful discussion and Dr Jim Zimbelman for his in-depth and valuable review.

References

Baker, V.R., 2001. Water and the martian landscape. Nature 412, 228-336.

Balme, M.R., Berman, D.C., Bourke, M.C., Zimbelman, J.R., 2008. Transverse aeolian ridges (TARs) on Mars. Geomorphology 101, 703-720.

Balme, M.R., Gallagher, C.J., 2009. An equatorial periglacial landscape on Mars. Earth and Planetary Science Letters 285, 1-15.

Balme, M.R., Mangold, N., Baratoux, D., Costard, F., Gosselin, M., Pinet, P., Neukum, G., 2006. Orientation and distribution of recent gullies in the southern hemisphere of Mars: Observations from High Resolution Stereo Camera/Mars Express (HRSC/MEX) and Mars Orbiter Camera/Mars Global Surveyor (MOC/MGS) data Camera/Mars Express (HRSC/MEX) and Mars Orbiter Camera/Mars Global Surveyor (MOC/MGS) data. Journal of Geophysical Research 111.

Berman, D.C., Balme, M.R., Rafkin, S.C.R., Zimbelman, J.R., 2011. Transverse aeolian ridges (TARs) on Mars II: distributions, orientations, and ages. Icarus 213, 116-130.

Bouley, S., Anson, V., Mangold, N., Masson, P., Neukum, G., 2009. Fluvial morphology of Naktong Vallis, Mars: A late activity with multiple processes. Planetary and Space Science 57, 982-999.

Bourke, M.C., Wilson, S.A., Zimbelman, J.R., 2003. The variability of transverse aeolian ridges in troughs on Mars. Lunar and Planetary Science XXXIV Abstract #2090.

Bradley, B.A., Sakimoto, S.E.H., Frey, H., Zimbelman, J.R., 2002. Medusae Fossae Formation: New perspectives from Mars Global Surveyor. Journal of Geophysical Research 107, 5058.

Breed, C.S., McCauley, J.F., Whitney, M.I., Tchakerian, V.P., Laity, J.E., 1997. Wind erosion in drylands, In: Thomas, D.S.G. (Ed.), Arid zone geomorphology. John Wiley & Sons, pp. 437-464.

Burr, D.M., Enga, M.-T., Williams, R.M.E., Zimbelman, J.R., Howard, A.D., Brenn, T.A., 2009. Pervasive aqueous paleoflow features in the Aeolis/Zephyria Plana region, Mars. Icarus 200, 52-73.

Burr, D.M., Williams, R.M.E., Wendell, K.D., Chojnacki, M., Emery, J.P., 2010. Inverted fluvial features in the Aeolis/Zephyria Plana region, Mars: Formation mechanism and initial paleodischarge estimates. Journal of Geophysical Research 115.

Calef, F.J., Herrick, R.R., Sharpton, V.L., 2009. Geomorphic analysis of small rayed craters on Mars: Examining primary versus secondary impacts. Journal of Geophysical Research 114.

Carr, M.H., 1995. The martian drainage system and the origin of valley networks and fretted channels. Journal of Geophysical Research 100, 7479-7507.

Carr, M.H., Malin, M.C., 2000. Meter-Scale Characteristics of Martian Channels and Valleys. Icarus 146, 366-386.

Carter, L.M., Campbell, B.A., Watters, T.R., Phillips, R.J., Puzig, N.E., Safaenili, A., Plaut, J.J., Okubo, C.H., Egan, A.F., Seu, R., Biccari, D., Orosei, R., 2009. Shallow radar (SHARAD) sounding observations of the Medusae Fossae Formation. Icarus 199, 295-302.

Clifford, S.M., Parker, T.J., 2001. The Evolution of the Martian Hydrosphere: Implications for the Fate of a Primordial Ocean and the Current State of the Northern Plains. Icarus 154,40–79.

Cutts, J.A., Smith, R.S.U., 1973. Aeolian deposits and dunes on Mars. Journal of Geophysical Research 78, 4139-4154.

de Silva, S.L., Bailey, J.E., Mandt, K.E., Viramonte, J.M., 2010. Yardangs in terrestrial ignimbrites: Synergistic remote and field observations on Earth with applications to Mars. Planetary and Space Science 58, 459-471.

DeHon, R.A., Washington, P.A., 2000. Implications of sapping channels on Mars. Lunar and Planetary Science XXXI Abstract #1147.

Dickson, J.L., Fassett, C.I., Head, J.W., 2009. Amazonian-aged fluvial valley systems in a climatic microenvironment on Mars: Melting of ice deposits on the interior of Lyot Crater. Geophysical Research Letters 36.

Easterbrook, D.J., 1999. Surface processes and landforms. Prentice Hall.

Edgett, K.S., Butler, B.J., Zimbelman, J.R., Hamilton, V.E., 1997. Geologic context of the Mars radar "Stealth" region in southwestern Tharsis. Journal of Geophysical Research 102, 21545-21568.

El Maary, M.R., Markiewicz, W.J., Mellon, M.T., Goetz, W., Dohm, J.M., Pack, A., 2010. Crater floor polygons: Desiccation patterns of ancient lakes on Mars? Journal of Geophysical Research 115.

Frey, H.V., Sakimoto, S.E.H., Roark, J.H., 1998. MOLA topography and stratigraphy of geologic units at the dichotomy boundary: The Medusae Fossae Formation. Lunar and Planetary Science XXIX Abstract #1619.

Goldspiel, J., Squyres, S.W., 2000. Groundwater sapping and valley formation on Mars. Icarus 148, 176-192.

Goudie, A.S., 2007. Mega-yardangs: A global analysis. Geography Compass 1/1, 65-81.

Greeley, R., Guest, J.E., 1987. Geologic map of the eastern equatorial region of Mars, Map I-1802-B.

Greeley, R., Iverson, J.D., 1985. Wind as a geological process on Earth, Mars, Venus and Titan. Cambridge University Press, Cambridge.

Guest, J.E., Murray, J.B., 1969. Nature and origin of Tsiolkovsky crater, lunar farside. Planetary and Space Science 17, 121-141.

Hardgrove, C., Whisner, S.C., Williams, R.M.E., Moersch, J.E., Chojnacki, M., Rogers, D., 2010. Remote thermophysical observations of terrestrial inverted relief features. Lunar and Planetary Science XLI Abstract #2497.

Harrison, S.K., Balme, M.R., Hagermann, A., Murray, J.B., Muller, J.-P., 2010. Mapping Medusae Fossae Formation materials in the southern highlands of Mars. Icarus 209, 405-415.

Head, J.W., 2001. Medusae Fossae Formation as ancient polar deposits?: Tests and new data on straigraphic relationships. Lunar and Planetary Science XXXII Abstract #1394.

Head, J.W., Kreslavsky, M.A., 2001. Medusae Fossae Formation as volatile-rich sediments deposited during high obliquity: An hypothesis and tests Conference on the Geophysical Detection of Subsurface Water on Mars Abstract #7053.

Head, J.W., Kreslavsky, M.A., 2004. Medusae Fossae Formation: Ice-rich airborne dust deposited during periods of high obliquity? . Lunar and Planetary Science XXXV Abstract #1635.

Hynek, B.M., Phillips, R.J., 2003. New data reveal mature, integrated drainage systems on Mars indicative of past precipitation Geology 31, 757-760.

Irwin, R.P., Howard, A.D., Craddock, R.A., 2008. Fluvial valley networks on Mars, In: Rice, S.P., Roy, A.G., Rhoads, B.L. (Eds.), River confluences, tributaries and the fluvial network. John Wiley & Sons Ltd.

Kerber, L., Head, J.W., 2009. The Age of the Medusae Fossae Formation: Evidence of Hesperian Emplacement from Crater Morphology, Stratigraphy, and Ancient Lava Contacts. Icarus 206, 669-684.

Kerber, L., Head, J.W., 2010. The age of the Medusae Fossae Formation: Evidence of Hesperian emplacement from crater morphology, stratigraphy and ancient lava contacts. Icarus 206, 669-684.

Keszthelyi, L., Jaeger, W.L., 2008. HiRISE observations of the Medusae Fossae Formation. Lunar and Planetary Science XXXIX Abstract #2420.

Keszthelyi, L., Thordarson, T., McEwen, A., Haack, H., Guilbard, M., Self, S., Rossi, M.J., 2004. Icelandic analogs to Martian flood lavas. Geochemistry Geophysics Geosystems 5.

Kneissl, T., Reiss, D., van Gasselt, S., Neukum, G., 2010. Distribution and orientation of northern-hemisphere gullies on Mars from the
evaluation of HRSC and MOC-NA data. Earth and Planetary Letters 294, 357-367.

Lefort, A., Burr, D., Beyer, R., Howard, A.D., 2012. Inverted fluvial features in the Aeolis-Zephyria Plana, western Medusae Fossae Formation, Mars: Evidence for post-formation modification. Journal of Geophysical Research 117.

Levy, J.S., Head, J.W., Marchant, D.R., Dickson, J.L., Morgan, G.A., 2009. Geologically recent gully–polygon relationships on Mars: Insights from the Antarctic Dry Valleys on the roles of permafrost, microclimates, and water sources for surface flow. Icarus 209, 113-126.

Malin, M.C., Bell, J.F., Cantor, B.A., Caplinger, M.A., Calvin, W.M., Clancy, R.T., Edgett, K.S., Edwards, L., Haberle, R.M., James, P.B., Lee, S.W., Ravine, M.A., Thomas, P.C., Wolff, M.J., 2007. Context Camera Investigation on board the Mars Reconnaissance Orbiter. Journal of Geophysical Research 112.

Malin, M.C., Edgett, K.S., 2000. Evidence for recent groundwater seepage and surface runoff on Mars. Science 288, 2330-2335.

Mandt, K.E., de Silva, S.L., Zimbleman, J.R., Crown, D.A., 2008. Origin of the Medusae Fossae Formation, Mars: Insights from a synoptic approach. Journal of Geophysical Research 113, E12011.

Mangold, N., 2005. High latitude patterned ground on Mars: Classification, distribution and climatic control. Icarus 174, 336-359.

McColley, S.M., Head, J.W., Neukum, G., 2005. The Medusae Fossae Formation: Geological characteristics and topographic and stratigraphic relationships of the lower member along southeastern Elysium Planitia. Lunar and Planetary Science XXXVI Abstract #1184.

McEwen, A.S., Eliason, E.M., Bergstrom, J.W., Bridges, N.T., Hansen, C.J., Delamere, W.A., Grant, J.A., Gulick, V.C., Herkenhoff, K.E., Keszthelyi, L., Kirk, R.L., Mellon, M.T., Squyres, S.W., Thomas, N., Weitz, C.M., 2007. Mars Reconnaissance Orbiter's High Resolution Imaging Science Experiment (HiRISE). Journal of Geophysical Research 112, 40.

McEwen, A.S., Preblich, B.S., Turtle, E.P., Artemieva, N.A., Golombek, M.P., Hurst, M., Kirk, R.L., Burr, D.M., Christensen, P.R., 2005. The rayed crater Zunil and interpretations of small impact craters on Mars. Icarus 176, 351-381.

Menzies, J., Shilts, W.W., 2002. Subglacial environments, In: Menzies, J. (Ed.), Modern and past glacial environments, pp. 183-278.

Morgan, G.A., Head, J.W., 2009. Sinton crater, Mars: Evidence for impact into a plateau icefield and melting to produce valley networks at the Hesperian–Amazonian boundary. Icarus 202, 39-59.

Pain, C.F., Clarke, J.D.A., Thomas, M., 2007. Inversion of relief on Mars. Icarus 190, 478-491.

Pain, C.F., Ollier, C.D., 1995a. Inversion of relief - a component of landscape evolution. Geomorphology 12, 151-165.

Pain, C.F., Ollier, C.D., 1995b. Inversion of relief: A component of landscape evolution. Geomorphology 12, 151-165.

Parker, T.J., 1991. A comparison of the Martian Medusae Fossae Formation with terrestrial carbonate platforms. Lunar and Planetary Science XXII 1029-1030.

Parker, T.J., 1994. Scientific rationale for selecting Northern Eumenides Dorsum (9deg-11degN latitude, 159deg-162deg longitude) as a potential Mars Pathfinder landing site. Mars Pathfinder Landing site workshop.

Ritter, D.F., Kochel, R.C., Miller, J.R., 2002. Process Geomorphology, 4th ed. Waveland Press Inc.

Scheidt, S.P., Zimbelman, J.R., 2011a. Preliminary geologic map of the MC-16 NW Quadrangle, Mars: Subdivisions of the lower and middle members of the Medusae Fossae Formation. Lunar and Planetary Science XLII Abstract #2631.

Scheidt, S.P., Zimbelman, J.R., 2011b. Preliminary geologic map of the MC-16 NW Quadrangle, Mars: Subdivisions of

the lower and middle members of the Medusae Fossae Formation. Lunar and Planetary Science XLII Abstract #2631.

Schmincke, H.-U., 1998. Volcanism. Springer.

Schultz, P.H., Lutz, A.B., 1988. Polar wandering on Mars. Icarus 73.

Scott, D.H., Tanaka, K.L., 1982. Ignimbrites of Amazonis Planitia Region of Mars. Journal of Geophysical Research 87, 1179-1190.

Scott, D.H., Tanaka, K.L., 1986. USGS Map I-1802-A.

Seibert, N.M., Kargel, J.S., 2001. Small-scale Martian polygonal terrain: Implications for liquid surface water. Geophysical Research Letters 28, 899-902.

Shockey, K.M., Zimbelman, J.R., Friedmann, S.J., Irwin, R.P., 2004. Geologic mapping of the Medusae Fossae Formation on Mars. Lunar and Planetary Science XXXV Abstract #1539.

Smith, D.E., Zuber, M.T., Solomon, S.C., Phillips, R.J., Head, J.W., Garvin, J.B., Banerdt, W.B., Muhleman, D.O., Pettengill, G.H., Neumann, G.A., Lemoine, F.G., Abshire, J.B., O., A., Brown, C.D., Hauck, S.A., Ivanov, A.B., McGovern, P.J., Zwally, H.J., Duxbury, T.C., 2000. The Global Topography of Mars and Implications for Surface Evolution. Science 284, 1495-1502.

Squyres, S.W., Knoll, A.H., Arvidson, R.E., Ashley, J.W., Bell, J.F.I., Calvin, W.M., Christensen, P.R., Clark, B.C., Cohen, B.A., de Souza, P.A.J., Edgar, L., Farrand, W.H., Fleischer, I., Gellert, R., Golombek, M.P., Grant, J., Grotzinger, J., Hayes, A., Herkenhoff, K.E., Johnson, J.R., Joliff, B., Klingelhofer, G., Knudson, A., Li, R., McCoy, T.J., McLennan, S.M.,

Ming, D.W., Mittlefeldt, D.W., Morris, R.V., Rice, J.W.J., Schroder, C., Sullivan, R.J., Yen, A., Yingst, R.A., 2009. Exploration of Victoria Crater by the Mars Rover opportunity. Science 324, 1058-1061.

Strahler, A.N., 1952. Hypsometric (area-altitude) analysis of erosional topography. Bulletin Geological Society of America 63, 1117-1142.

Tanaka, K.L., 2000. Dust and ice deposition in the Martian geologic record. Icarus 144, 254-266

Todd, D.K., Mays, L.W., 2005. Groundwater Hydrology, 3rd ed. Wiley.

Watters, T.R., Campbell, B., Carter, L., Leuschen, C.J., Plaut, J.J., Picardi, G., Orosei, R., Safaeinili, A., Clifford, S.M., Farrell, W.M., Ivanov, A.B., Phillips, R.J., Stofan, E.R., 2007a. Radar sounding of the Medusae Fossae Formation Mars: Equatorial ice or dry, low-density deposits? Science 318, 1125-1128.

Watters, T.R., Campbell, B.A., Carter, L.M., Leuschen, C.J., Plaut, J.J., Picardi, G., Safaeinili, A., Clifford, S.M., Farrell, W.M., Ivanov, A.B., Phillips, R.J., Stofan, E., Team, t.M.S., 2007b. MARSIS subsurface radar sounding of the Medusae Fossae Formation, Mars. Lunar and Planetary Science XXXVIII Abstract #1661.

Wentworth, S.J., Gibson, E.K., Velbel, M.A., McKay, D.S., 2005. Antarctic Dry Valleys and indigenous weathering in Mars meteorites: Implications for water and life on Mars. Icarus 174, 383-395.

Williams, R.M.E., Irwin, R.P., Zimbelman, J.R., 2009. Evaluation of paleohydrologic models for terrestrial inverted channels: Implications for application to martian sinuous ridges. Geomorphology 107, 300-315.

Williams, R.M.E., Irwin, R.P., Zimbelman, J.R., Chidsey, T.C., Eby, D.E., 2011. Field guide to exhumed paleochannels near Green River, Utah: Terrestrial analogs for sinuous ridges on Mars, In: Garry, W.B., Bleacher, J.E. (Eds.), Analogs for Planetary Exploration. Geological Society of America pp. 483-505.

Wilson, L., Head, J. W., 2009. Tephra deposition on glaciers and ice sheets on Mars: Influence on ice survival, debris content and flow behaviour. Journal of Volcanology and Geothermal Research 185, 290-297.

Zimbelman, J.R., 2010. Geologic mapping of the MC-23 NW Quadrangle: Emplacement and erosion of the lower member of the Medusae Fossae Formation on Mars. Lunar and Planetary Science XLI Abstract #1157.

Zimbelman, J.R., Griffin, L.J., 2010. HiRISE images of yardangs and sinuous ridges in the lower member of the Medusae Fossae Formation, Mars. Icarus 205, 198-210.

Zimbelman, J.R., Crown, D., Jenson, D., 1996. Initial investigation of the enigmatic massive deposits in Amazonis Planitia, Mars. Lunar and Planetary Science XXVII Abstract #1748.

Zimbelman, J.R., Crown, D.A., Grant, J.A., Hooper, D.M., 1997. The Medusae Fossae Formation, Amazonis Planitia, Mars: Evaluation of proposed hypotheses of origin. Lunar and Planetary Science XXVIII Abstract #1482.

Zimbelman, J.R., Hooper, D., Crown, D., Grant, J., Sakimoto, S.E.H., Frey, H., 1999. Medusae Fossae Formation, Mars: An assessment of possible origins utilising early results from Mars Global Surveyor. Lunar and Planetary Science XXX Abstract #1652.

Zimbelman, J.R., Scheidt, S.P., 2012. Hesperian Age for Western Medusae Fossae Formation, Mars. Science 336.

Figure captions:

Figure 1: Overview of the study area. Note branching ridge system in the southern depression and the dark mantling material in the northwest of the northern crater. (CTX image P16_007394_1748_XN_05S180W, HiRISE images PSP_007394_1750 and PSP_008185_1750). Image credits: NASA/JPL/MSSS and NASA/JPL/Univ. Arizona.

Figure 2: Regional context of the Medusae Fossae Formation with individual lobes A, B, C, D and E labelled. The Crustal Dichotomy Boundary and two largest volcanoes of the region are also labeled. Base map is MOLA global digital elevation model overlain upon a THEMIS daytime infrared mosaic of 512 pixels per degree. Lighter toned regions are topographically higher. Data credit: MOLA science team; NASA/JPL/ASU).

Figure 3: The central lobe of the MFF (Lobe C in Fig. 2). The local context for the study area described in this paper is shown by the black box. Base map is MOLA global DEM layered over a THEMIS day infrared mosaic of 512 ppd. Image credit: MOLA science team; NASA/JPL/ASU.

Figure 4: Example of surface textures of the middle member exposure in the lobe on which the study area is present (CTX P16_007394_1748). Note the highly degraded surfaces, with few, if any, features that can reliably be identified as yardangs. Image credit NASA/JPL/MSSS.

Figure 5: Simple geomorphological map of the study area showing the main features. Non-shaded areas are interpreted to be Medusae Fossae Formation materials. The dominant features are the materials which comprise the branching network and which also (re)surface the northern crater floor, and the dark mantling materials which cover the western parts of the crater floor.

Figure 6: Example of the upper surface of larger branches from the dendritic network. Note mesa-like projections at the left of the image and linear ridges in the center, both of which appear to be integral to the network material. Note also how the cracks in the surface postdate these features and many of the craters, with the notable exception of a small crater with raised ejecta (arrowed). Image credit: HiRISE PSP_007394_1750, NASA/JPL/Univ. Arizona.

Figure 7: Linear cracking on the surface of the inverted channel fill. Note how the cracks follow the bifurcation angle. The top image provides context within the network. Image credit: HiRISE PSP_007394_1750, NASA/JPL/Univ. Arizona.

Figure 8: Portions of two first order branches, which at regional scale exhibit apparently straightforward ridge-like morphology, but which at full HiRISE resolution are more complex. a) A portion of a branch, with layered margins (i), and another area that has a gentle slope to one side, almost merging into the depression floor (ii). b) a portion of a branch where the ridges appear flattened, and seem to rise from the depression floor itself. Image credit: HiRISE PSP_007394_1750 and PSP_008185_1750, NASA/JPL/Univ. Arizona

Figure 9: Small, narrow ridges (shown by the arrows) occurring on top of a first order branch of the larger network. Image credit: HiRISE PSP_007394_1750, NASA/JPL/Univ. Arizona

Figure 10: Stepped edge of the inverted network indicating either (i) layers of differing strength or lithology, or (ii) horizontal planes of weakness. Correspondent to this are what appear to be yardangs away from the inverted network that seem to have tops on similar planes to the network layers. Image credit: HiRISE PSP_008185_1750, NASA/JPL/Univ. Arizona.

Figure 11: Example of first order branches corresponding with scalloped depression edges. This could represent an association between ridge initiation and erosional headscarps. Note that the base of the scarps are now covered by debris and what appear to be aeolian deposits. Image credit: HiRISE PSP_007394_1750 and CTX P16_007394_1748_XN_05S180W, NASA/JPL/Univ. Arizona and NASA/JPL/MSSS.

Figure 12: Apparent contact between two layers (shown by the arrows) in the depression cliff edge. A darker, thinner top layer overlays a lighter, thicker lower layer. The occurrence of boulders and talus at the base of the slopes indicate failure of the cliff material and active mass wasting processes, probably in some part due to differential erosion of the two differing layers. Image credit: HiRISE PSP_008185_1750, NASA/JPL/Univ. Arizona.

Figure 13: Example of mantling deposits near the contact between the middle and upper members, on the MFF lobe ~ 50 km south of the crater-channel system. These deposits are very similar in morphology to those which occur on the western parts of the crater and depression floors. Portion of CTX image P16_007394_1748_XN_05S180W. Image credit: NASA/JPL/MSSS.

Figure 14: Detail of low albedo mantling deposits. A short (~10 m) wavelength pattern of NE-SW trending lineaments is set over a larger (50-100 m) wavelength background texture. Note the apparent ripple-like morphology of the smallest forms, which appear to be TARs. Note that this does not necessarily mean that the larger forms, or the whole deposit, are aeolian as the TARs

could be reworked material from the deposit. Image credit. Part of HiRISE image PSP_008185_1750. Image credit: NASA/JPL/Univ. Arizona.

Figure 15: Example of surface textures in the 'fan', immediately north of the margin between the crater and the depression, extending up to 7 km from the breach. In the center and east of the image can be seen what appears to be inverted braiding This area is inferred to represent the depositional portion of the fluvial system which both created the fan-shaped form and which resurfaced the northern crater floor. Image credit: HiRISE PSP_008185_1750, NASA/JPL/Univ. Arizona.

Figure 16: Region of well-defined layering and mesas in the crater floor surface. The positive topographic relief structures have distinctive curved edges and stepped margins. This is inferred to represent the differential erosion of distinct layers within this material, which may correspond with those observed in the inverted ridge network to the south (Fig. 10). Image credit: HiRISE PSP_008185_1750, NASA/JPL/Univ. Arizona.

Figure 17: Pattern of albedo 'swirls' in the crater floor surface, as visible in CTX images. The northern edge of the HiRISE image can be seen at the bottom of the figure covering the furthest southern extent of this swirl surface. What can be seen of this surface in the HiRISE images appears to show the swirl pattern is the result of layering and erosion within the surface material. Image credits: HiRISE PSP_008185_1750 and CTX P16_007394_1748_XN_05S180W, NASA/JPL/Univ. Arizona and NASA/JPL/MSSS.

Figure 18: Faint polygonisation patterns at roughly meter to decameter-scale, occuring in the floor of the northern crater. Image credits: HiRISE PSP_008185_1750, NASA/JPL/Univ. Arizona.

Figure 19: Yardangs on the depression floor that appear to be eroding out from the inverted network itself. These yardangs have morphology similar to MFF materials elsewhere in the formation. Image credit: HiRISE PSP_007394_1750 and HiRISE PSP_007394_1750, NASA/JPL/Univ. Arizona.

Figure 20: Individual small to mesoscale yardangs (< 100 m) occurring on top of the surface of the inverted network. Thiese could be the last remnants of a continuous layer that has undergone almost complete deflation.. Image credit: HiRISE PSP_007394_1750, NASA/JPL/Univ. Arizona.

Figure 21: Putative inverted crater fill ~ 50 m across, in the west of the crater floor surface, proximal to the edge of the mantling deposits. This feature shows distinct layering, which may correspond to the layering observed to the east in the crater floor. Note polygonisation similar to that shown in Fig. 18 but which has a radial and circumferential pattern, probably caused by association with the crater. Image credit: HiRISE PSP_007394_1750, NASA/JPL/Univ. Arizona.

Figure 22: a - Raised ejecta craters, numbering more than 6, in the northeast area of albedo 'swirl' area. Note the consistent axis of asymmetry, with the width of the ejecta being greatest to the NE and SW, and narrowest to the NW, giving a 'butterfly' type morphology. Portions of the 'swirl' material are readily identifiable. Image credits: CTX P16_007394_1748_XN_05S180W, NASA/JPL/MSSS. b- Raised-ejecta crater on the surface of the inverted network. The ejecta has an asymetrical morphology with 'wings' to the NE and SW, extending up to 280 m from the crater rim (outlined). This morphology reflects that shown by small impact craters in the northern crater. Note post impact cracking on the ejecta, and that this example is the only one of its kind on the surface of the channel network itself. Image credit: HiRISE PSP_007394_1750, NASA/JPL/Univ. Arizona.

Figure 23: Distribution of the MOLA raw data points across the study area. This demonstrates the gaps in the data coverage at this scale, which result in significant portions of the gridded MOLA DEM of this area being derived solely from interpolation of the surrounding points. Data credit: MOLA science team

Figure 24: 3-D hillshaded visualization of the DTM derived from the CTX stereo pair using the Ames Stereo Pipeline (Moratto, 2011). This perspective highlights the significant differences between the floor heights of the crater and depression, the mantling unit of the crater in the northwest, and the nature of the branched network.

Figure 25: a - S-N profiles across the study area (as shown in context image c). The 'breach' area between the southern depression and northern crater is clearly identifiable, as are the branches of the inverted network rising above the depression floor. The local slope clearly shows the considerable difference in the base levels of the northern crater and the southern depression. Note that profiles 1-3 follow MOLA tracks, but profile 4 does not, so has larger interpolation errors. b – W-E profiles across the study area (as shown in context image c). The east of the crater is deeper than the west, which appears to be due to the low albedo mantling deposits in the west. The roughly 100 m increase in depth to the east within the depression is attributed to either infill, uneven exhumation, or a combination of the two. The inverted branches on the depression floor are clearly identifiable in profile 2 as are the relatively steep scarps of the depression margins.

Figure 26: Longitudinal profiles drawn along three branches of the inverted network, as shown in context image to the right. The CTX DEM elevation values have been corrected to the MOLA data points and use a 20 point moving average smooth on the raw data, which were sampled every few meters. A general negative downstream slope trend can be observed in branch 1and

along the main trunk itself. The eastern,branch 2 is not only topographically lower but appears to be lower in the middle of the branch than where it meets the main trunk..

Figure 27: Cross-section profiles of the inverted network (shown in context in subset). From south to north, the main branch becomes wider and flatter, culminating in the broad, very flat area before the breach into the northern crater. Note that the furthest western elevations are consistently higher than the eastern, which matches the increased depth of the depression in the eastern portions. This might suggest that the whole region has tilted slightly, or that deflation occurred preferentially on the western side of a given topographic obstacle.

Figure 28: Distribution of network width:height ratios with distance along the network. The lower order branch section of the main trunk shows the highest ratios, with a fairly consistent negative trend along the rest of the length.

Figure 29. Regional topography and geology of the middle lobe of the MFF in which the study area occurs. a – topographic map of the lobe showing position of profile AA'. White box shows approximate location of figure 1. b – geological map (after Greeley and Guest 1987, Scott and Tanaka, 1986) of the same location showing the positions of the lower (Aml), middle (Amm) and upper (Amu) members of the MFF. c- topographic profile from MOLA data showing position of unit boundaries and inferred cross section (assuming horizontal layering). The position of the crater and depression along the profile is shown by the shaded area.

Figure 30: An SR feature in the western MFF, shown in local context (a) and close-up (b), previously described in Burr et al. (2009). Burr et al. classified this as a multilevel SR, associated with a fan shape. They interpreted it as a water-lain feature. Image credit: CTX image P21_009109_179, NASA/JPL/MSSS.

Figure 31: Diagram showing a proposed linear sapping model for the evolution of the branched network and associated depression. a - Melt initiates at impact crater margin; sapping process initiates headward erosion, b - Continuing headward erosion begins to form a depression with scalloped headscarps, c - Sapping flow undermines the material above, causing collapse; materials are carried into northern crater, resurfacing the floor. Channel is subsequently armored and then buried. d - Aeolian deflation later exposes the relict form.

Figure 32: Diagram showing a proposed centripetal sapping model for the evolution of the branched network and associated depression. a - Impact generates melt of ground ice, initiating a centripetal sapping flow, b - Continuing centripetal sapping begins to modify the crater edges to form scalloped headscarps, c - Headward erosion breaches rim of crater to the N; base level lowers and flow essentially reverses flow back into the crater, resurfacing the floor. Channel is subsequently armored and then buried. d - Aeolian deflation later exposes the relict form.

Highlights

- Observation and analysis of a branching positive relief system
- Quantitative analysis conducted using a ~15 m per pixel CTX DTM
- Evidence suggests that this inverted form was once a fluvial system
- After evaluation of possible origins, seepage sapping is suggested the most likely
- Some portions of the Medusae Fossae Formation may be volatile-rich

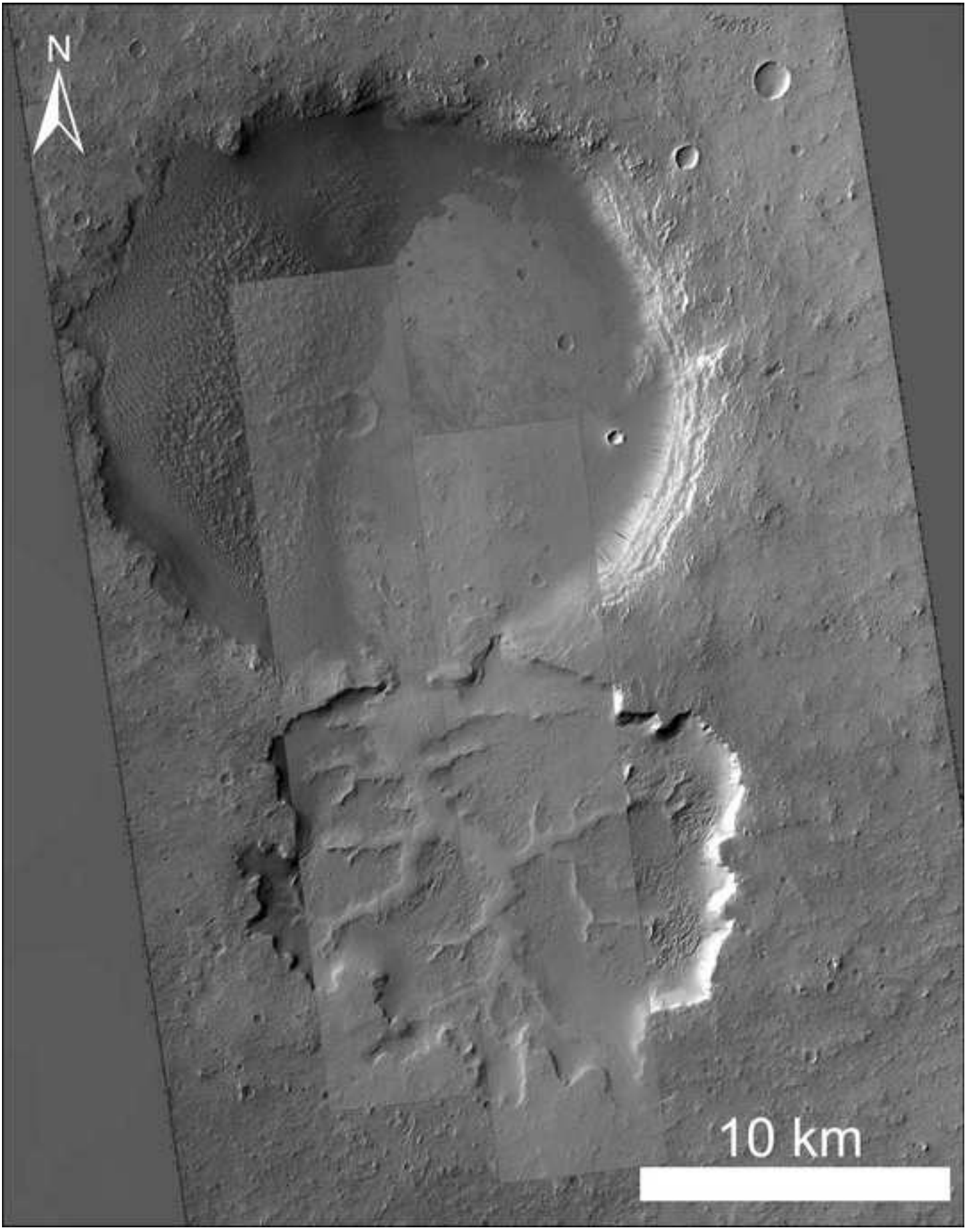

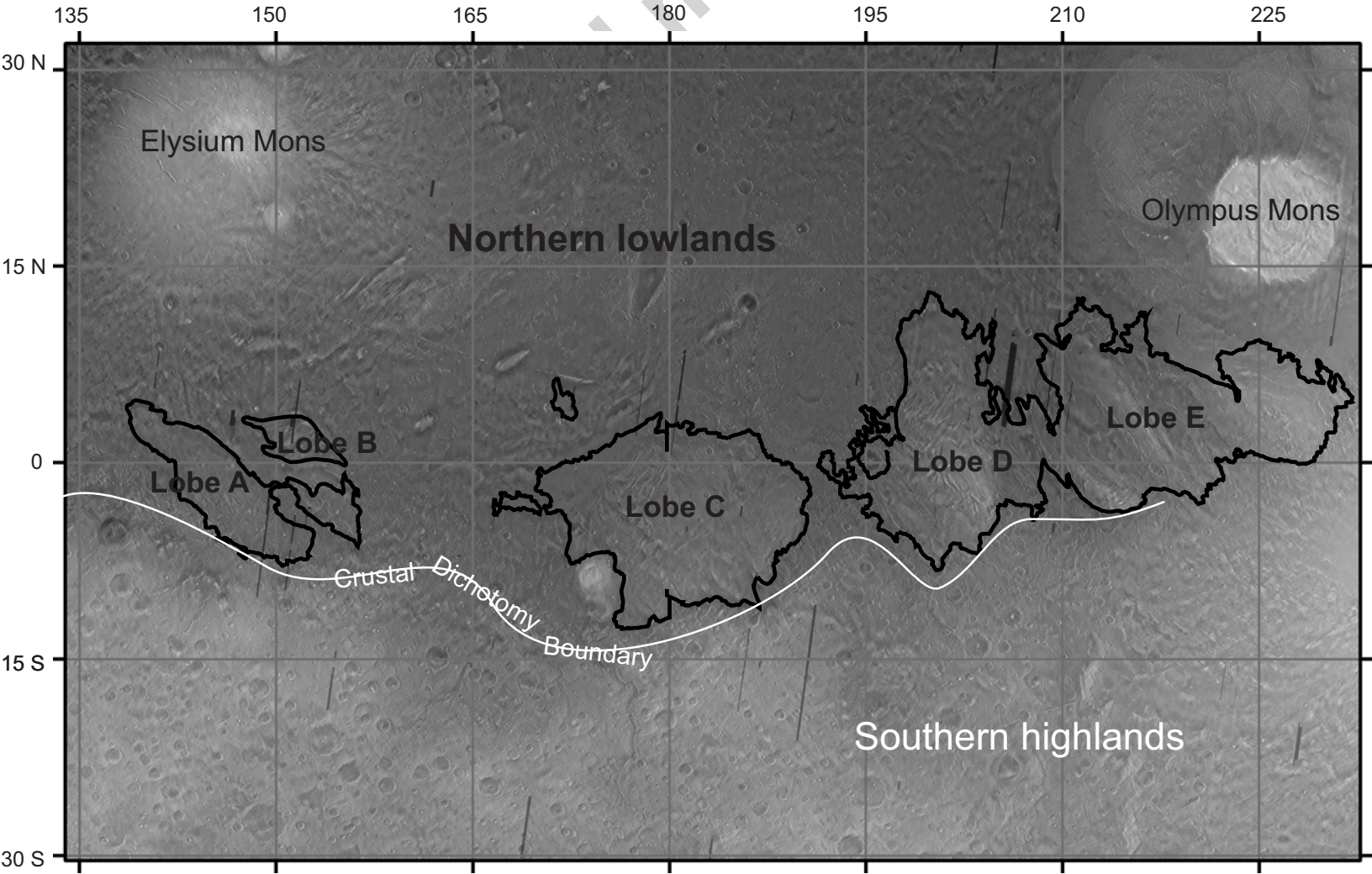

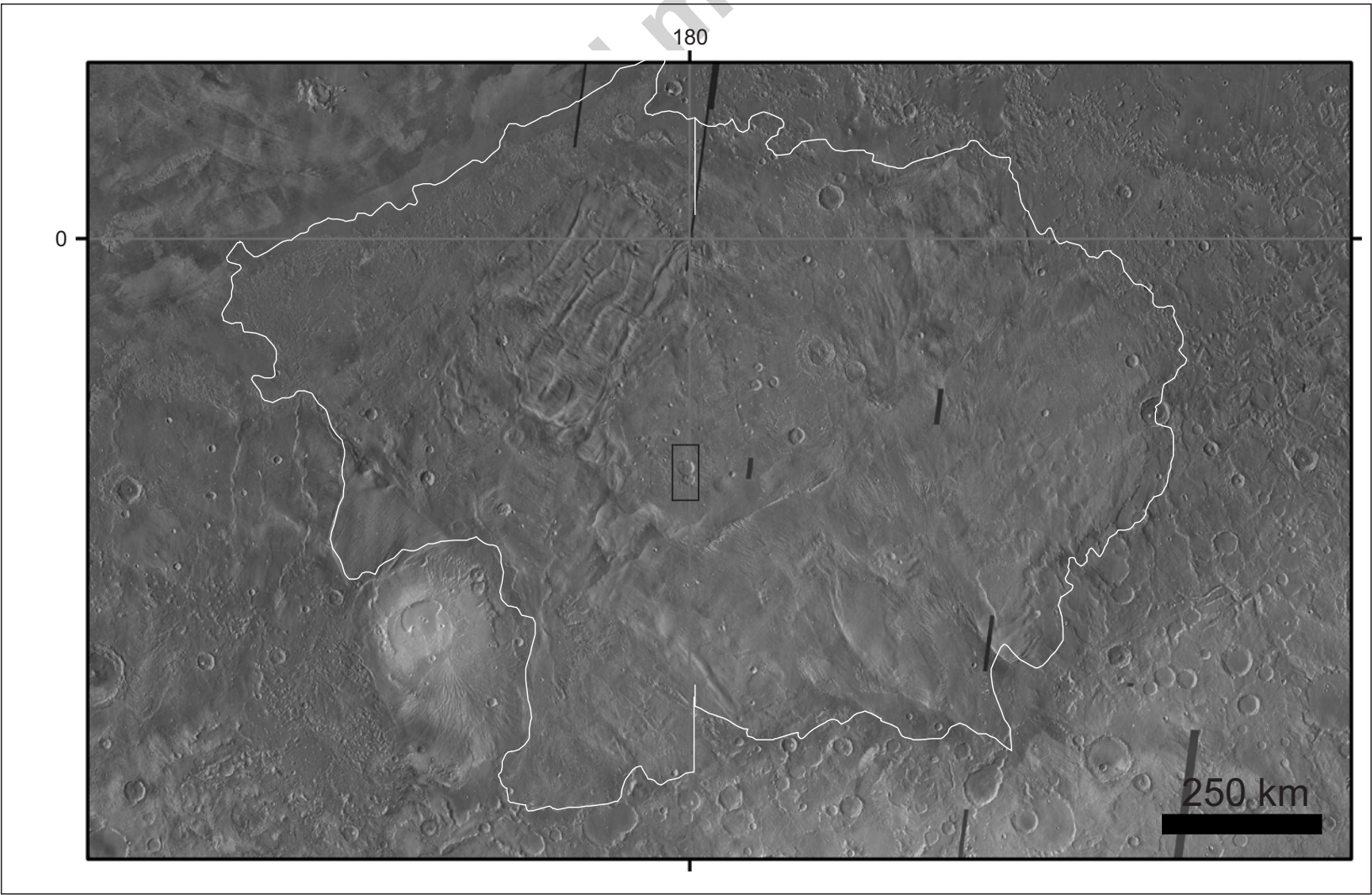

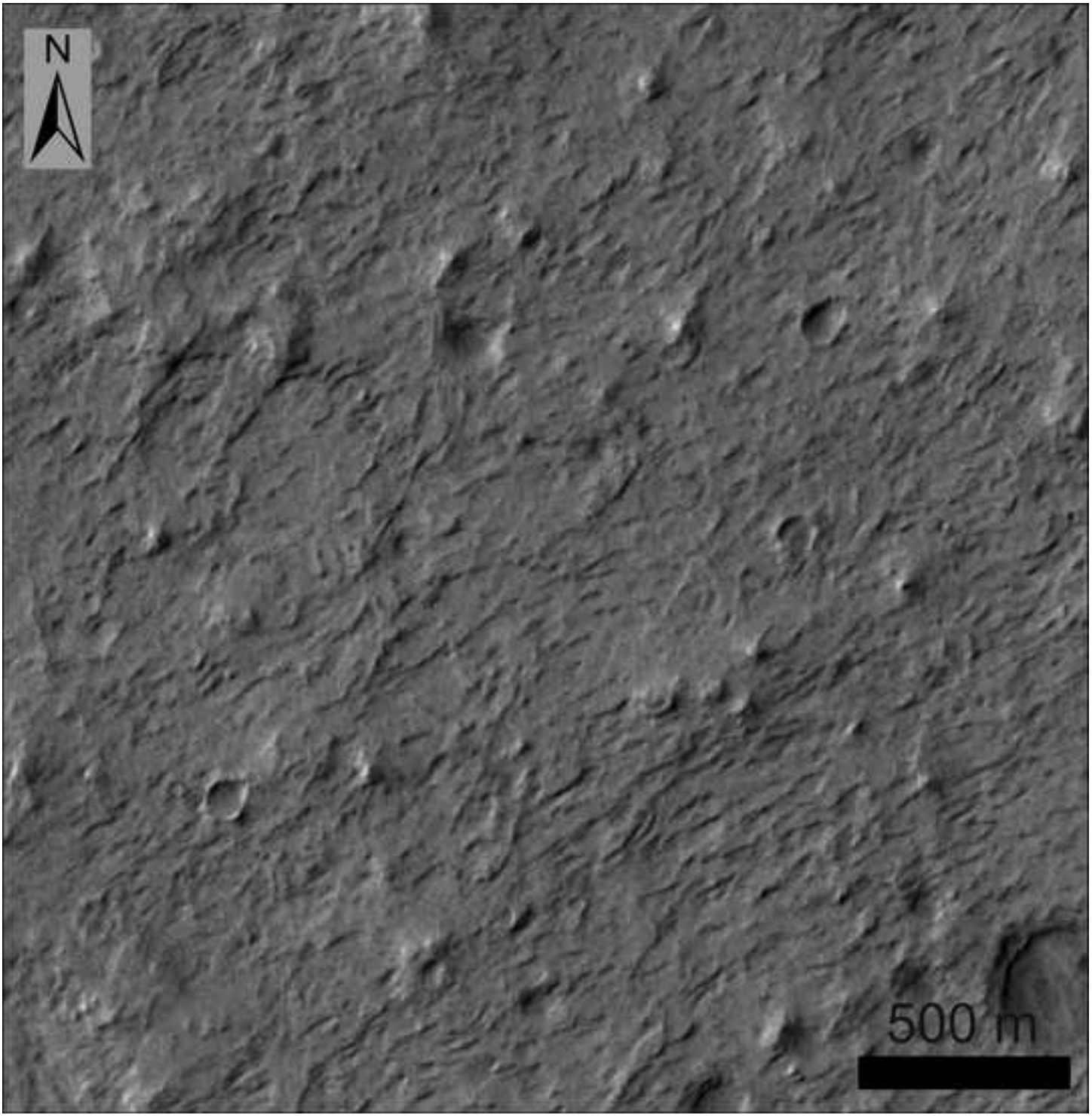

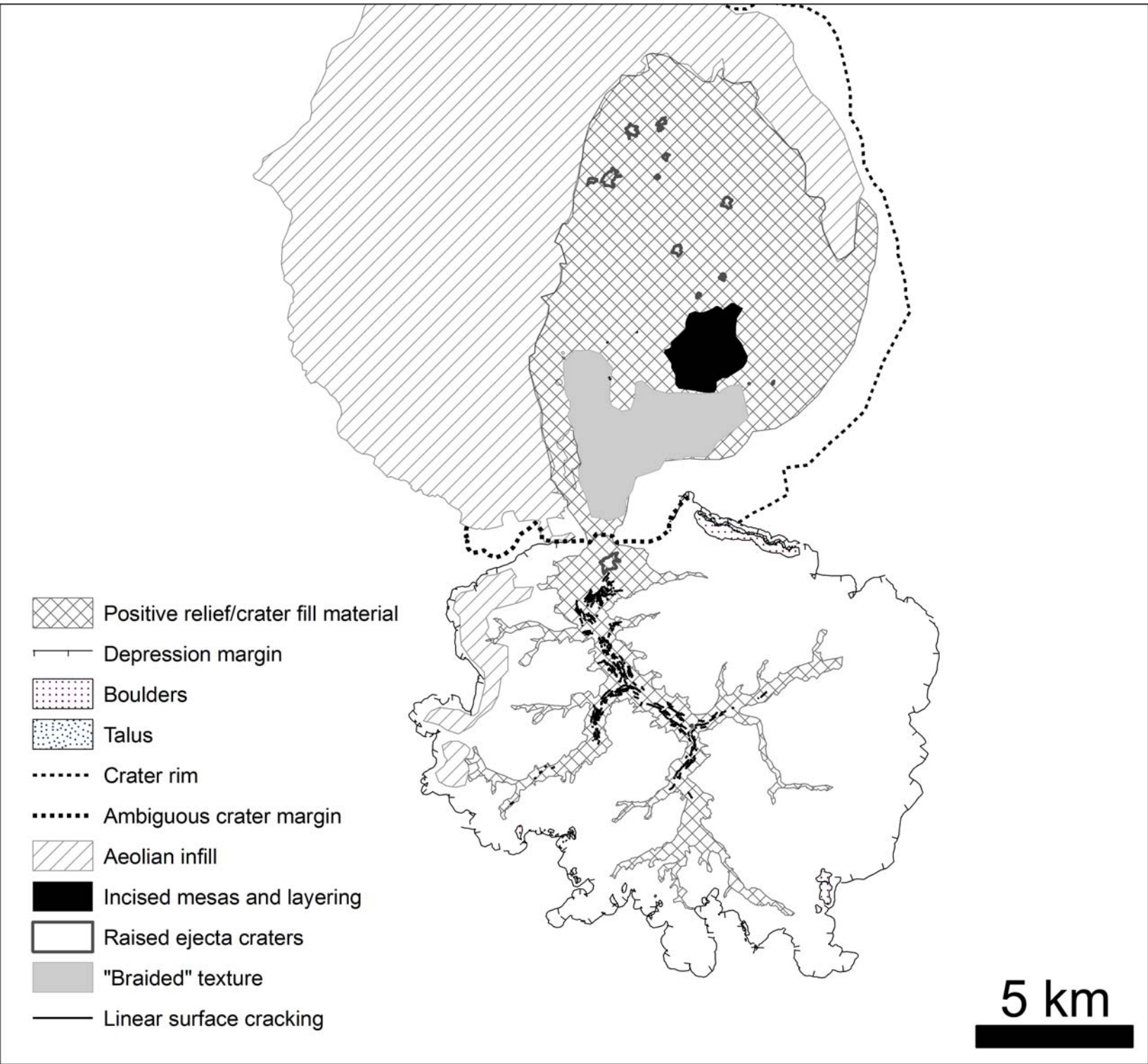

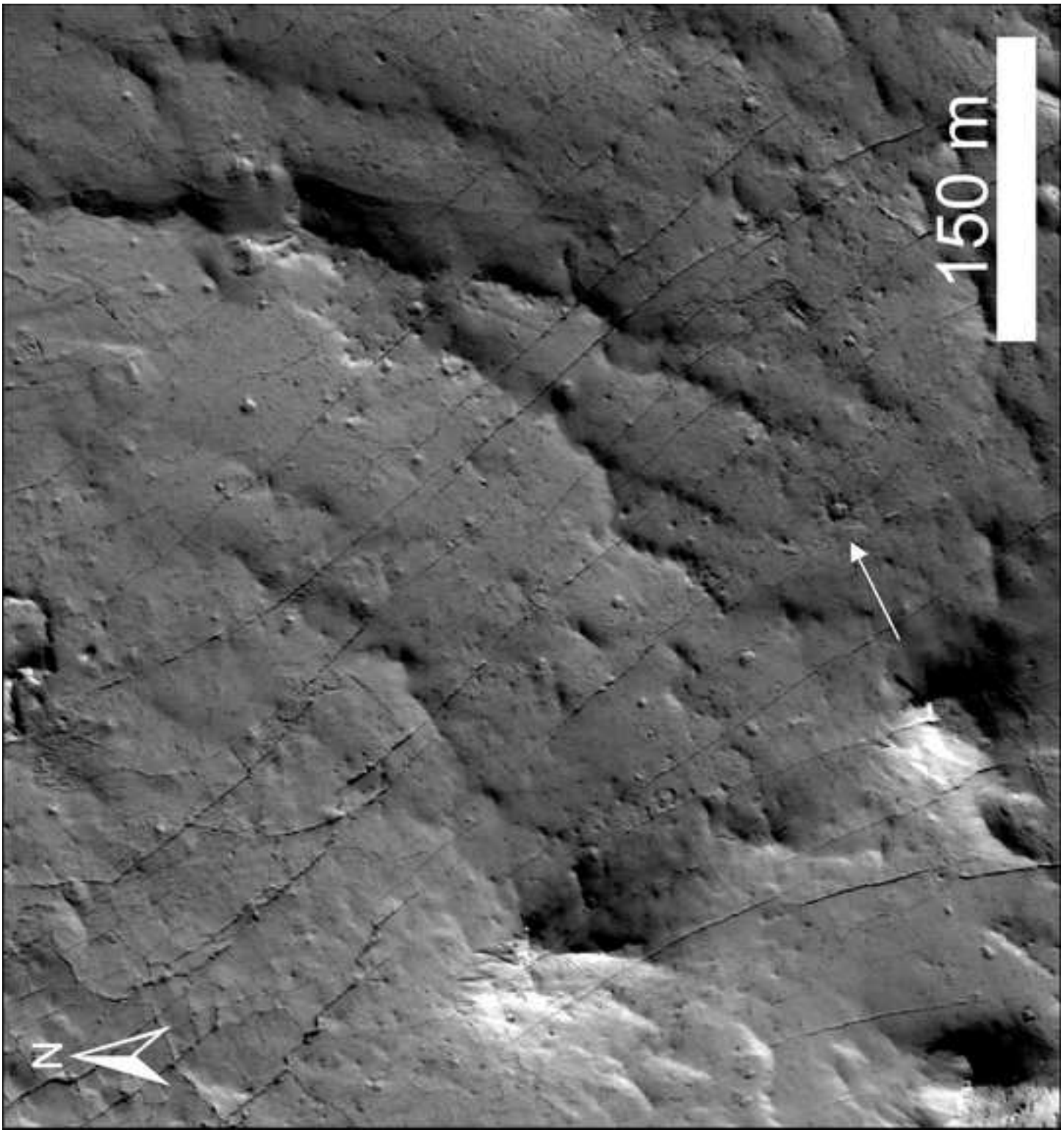

Figure

Figure

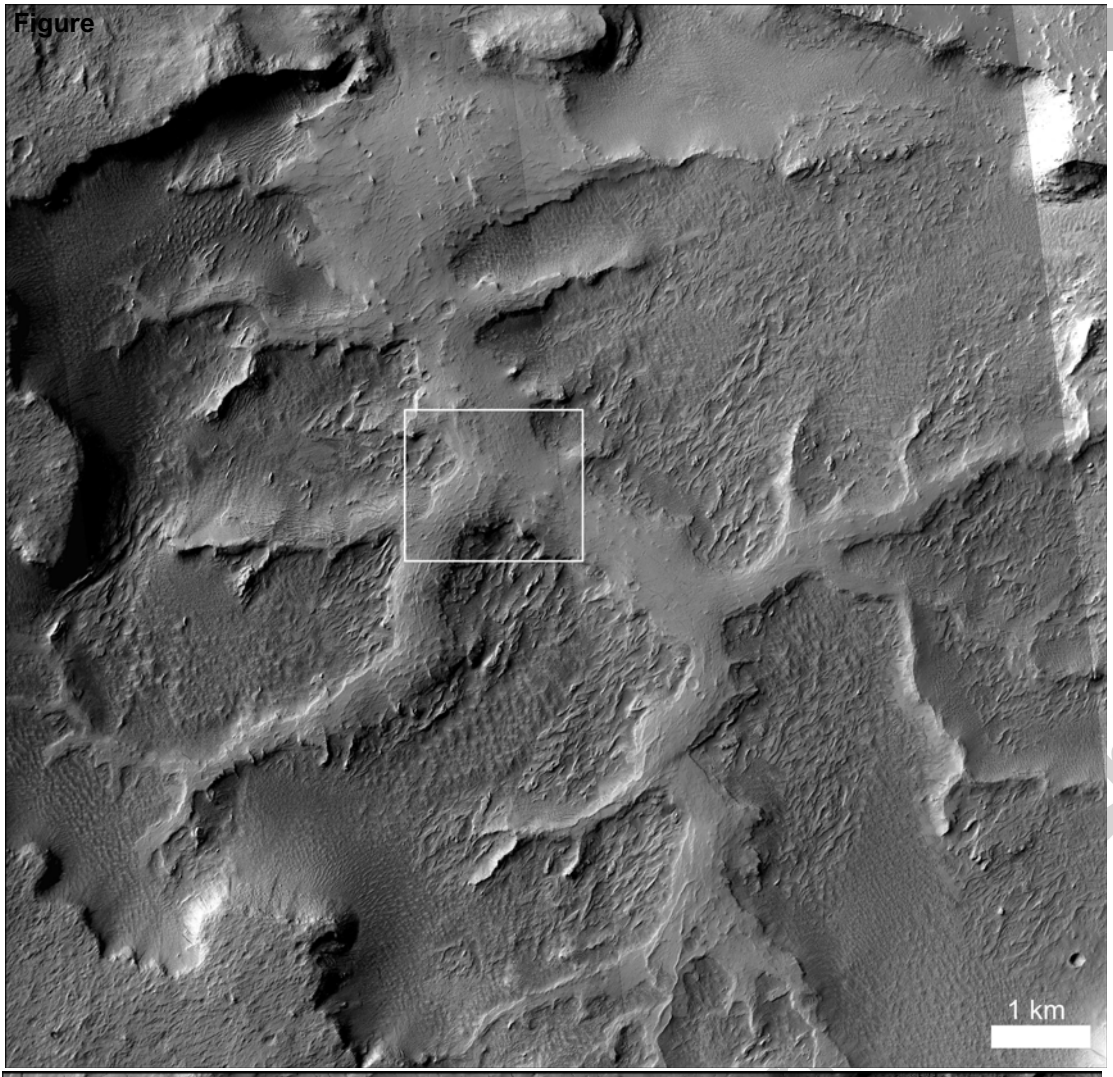

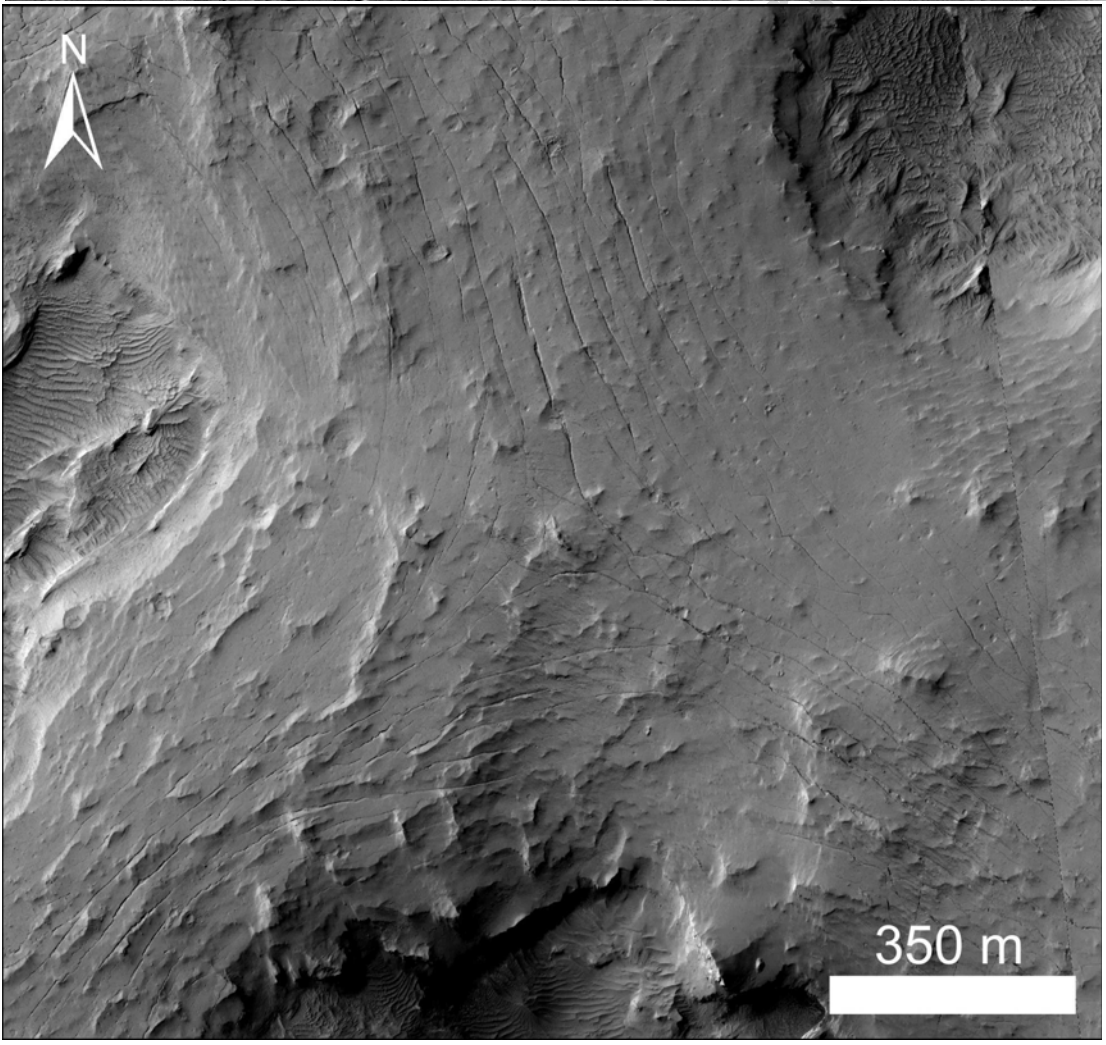

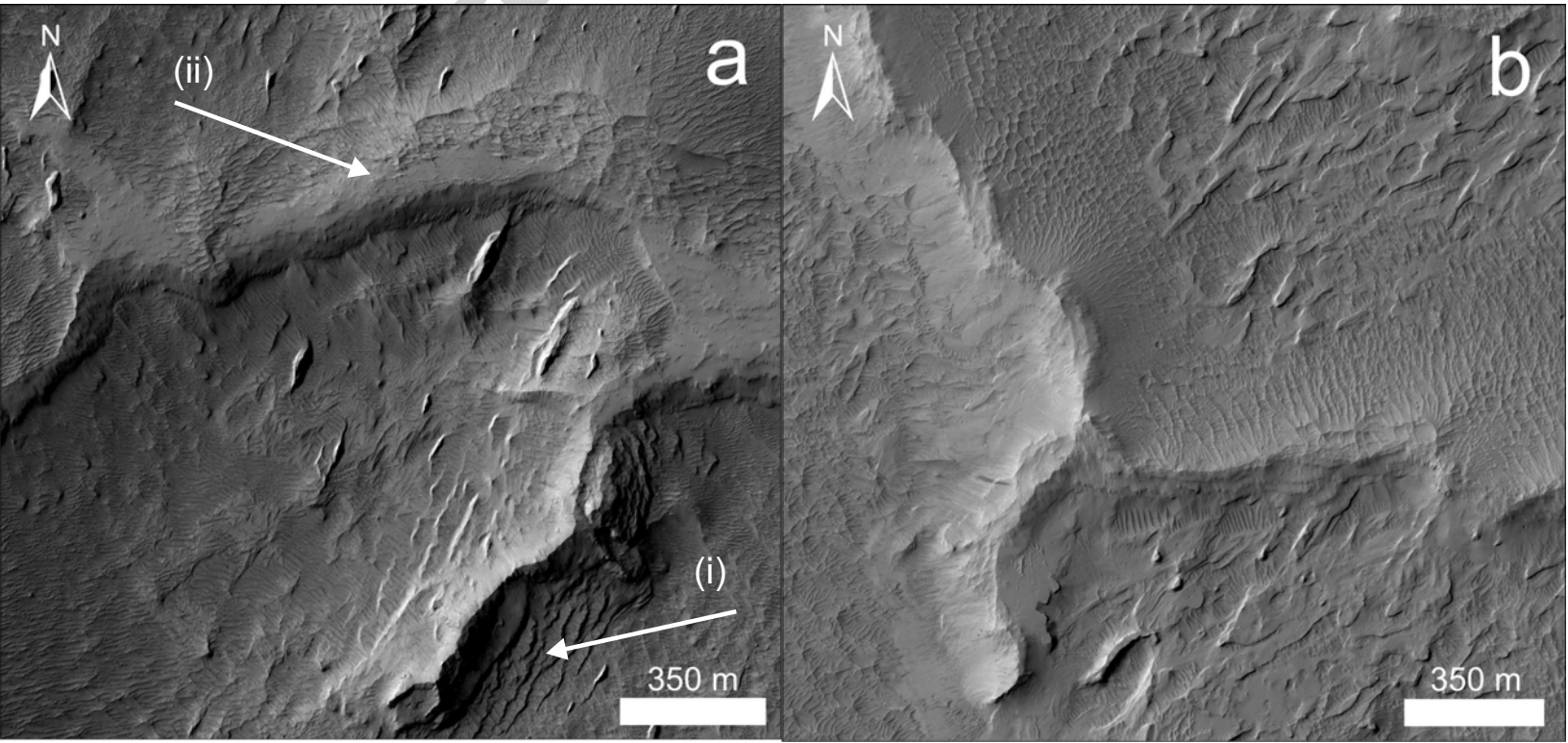

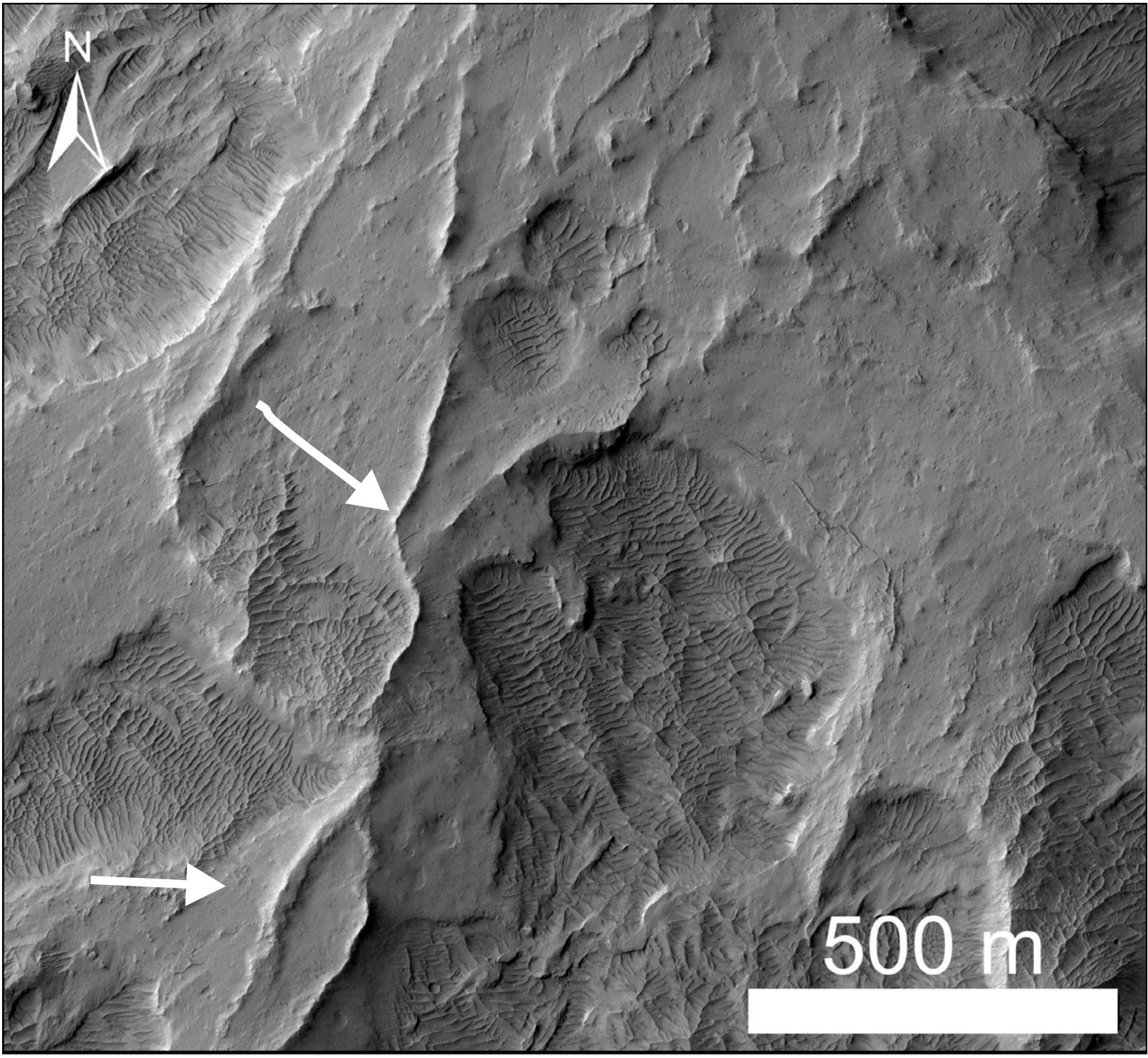

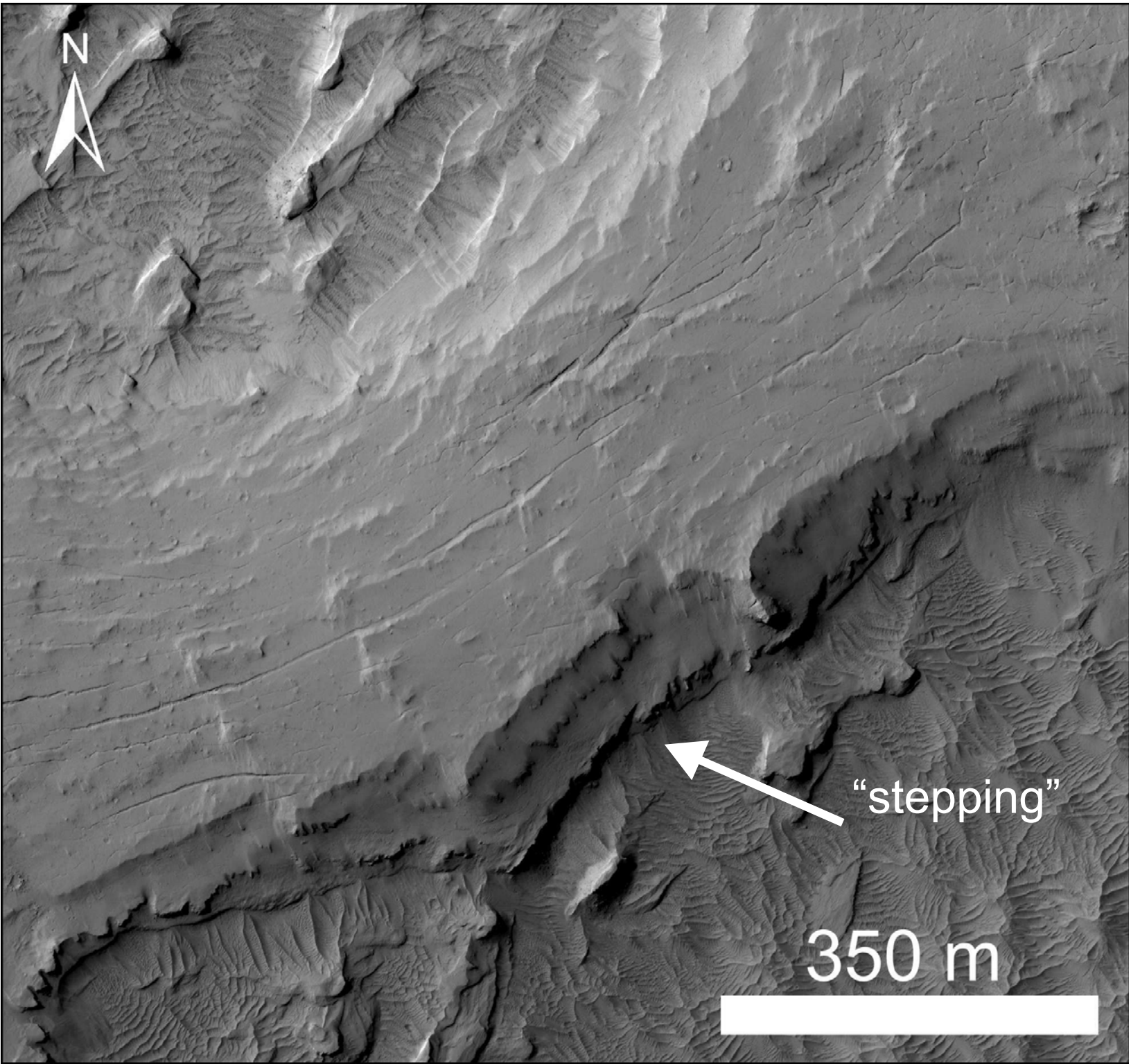

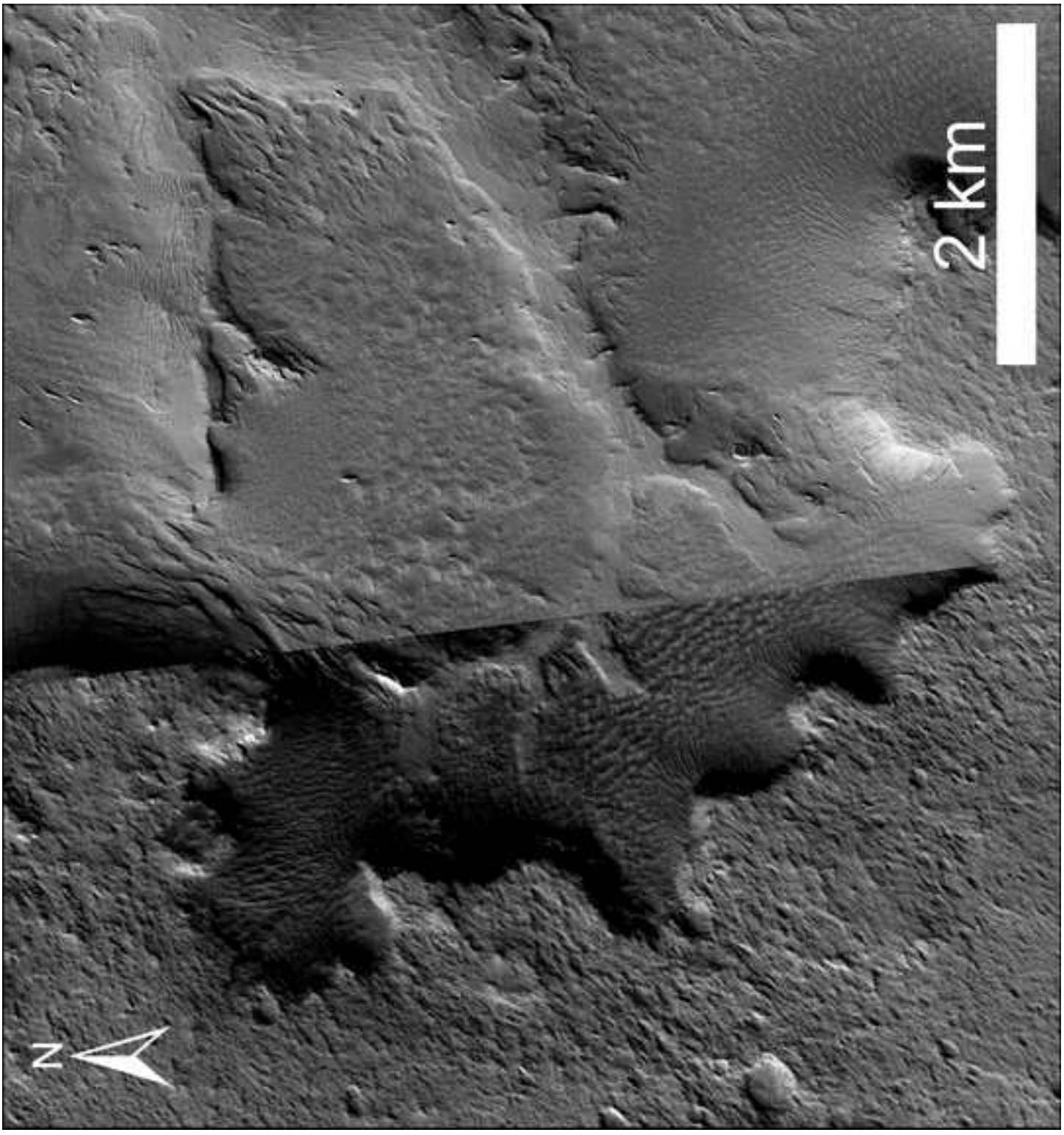

Figure

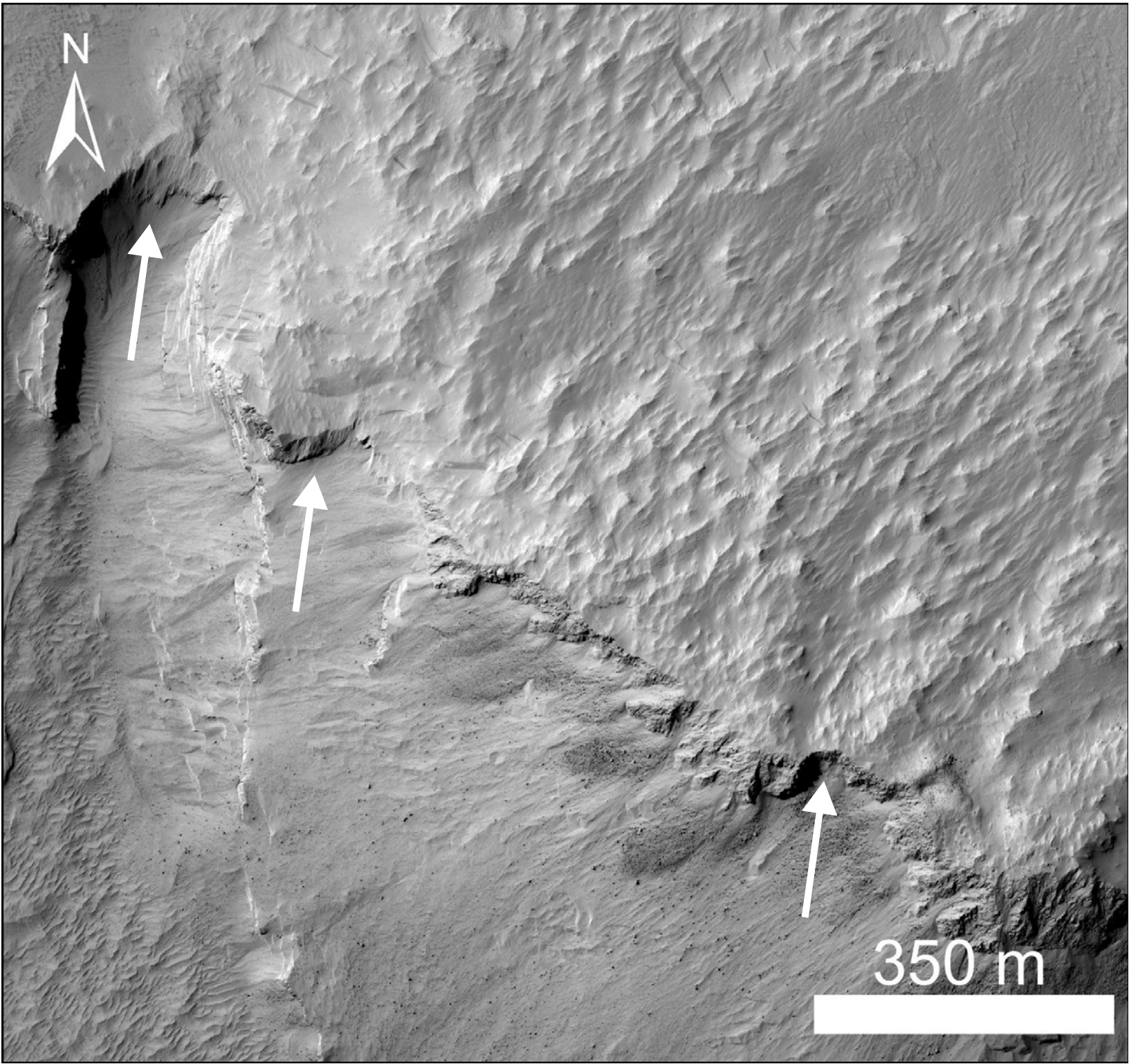

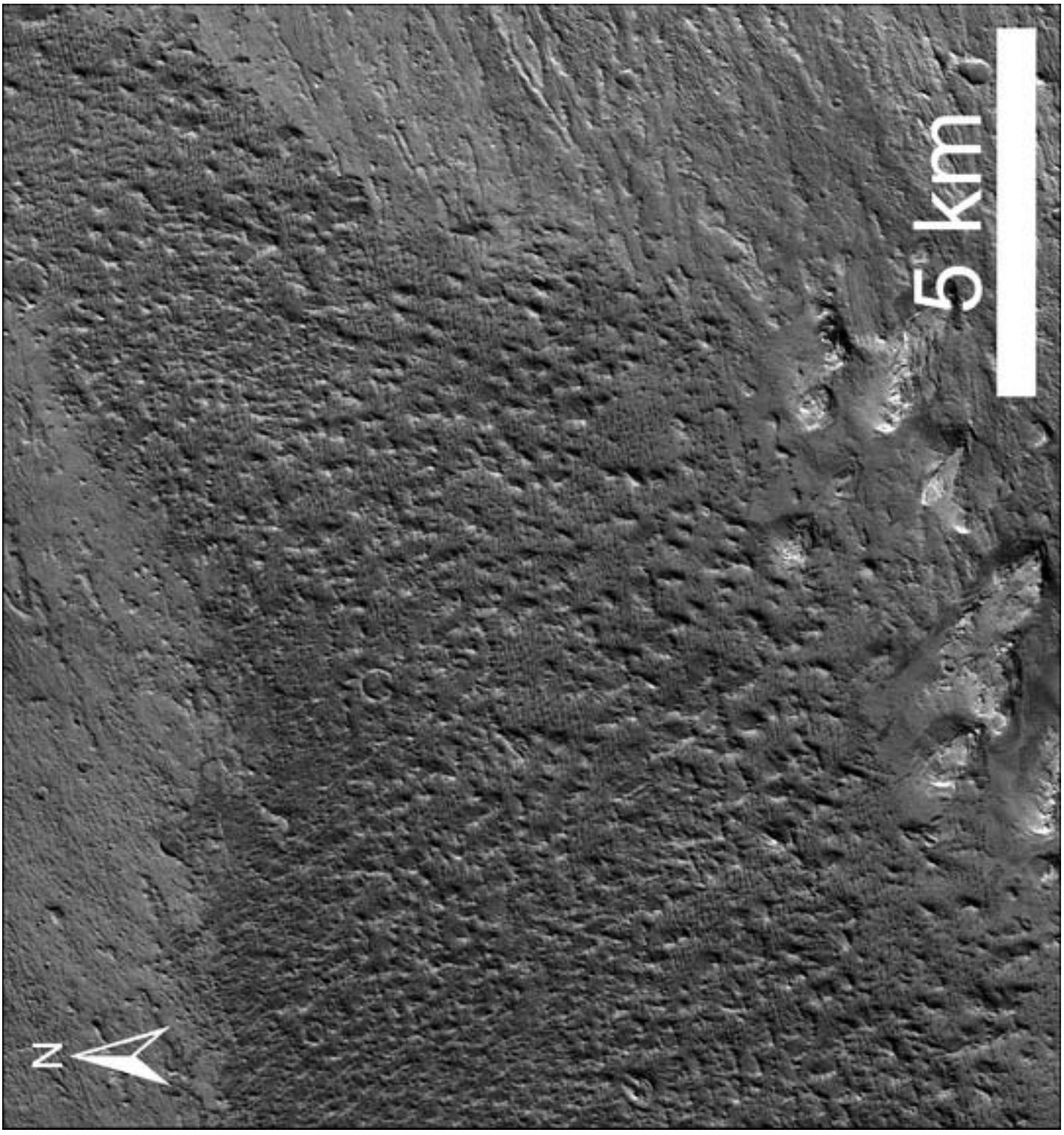

Figure

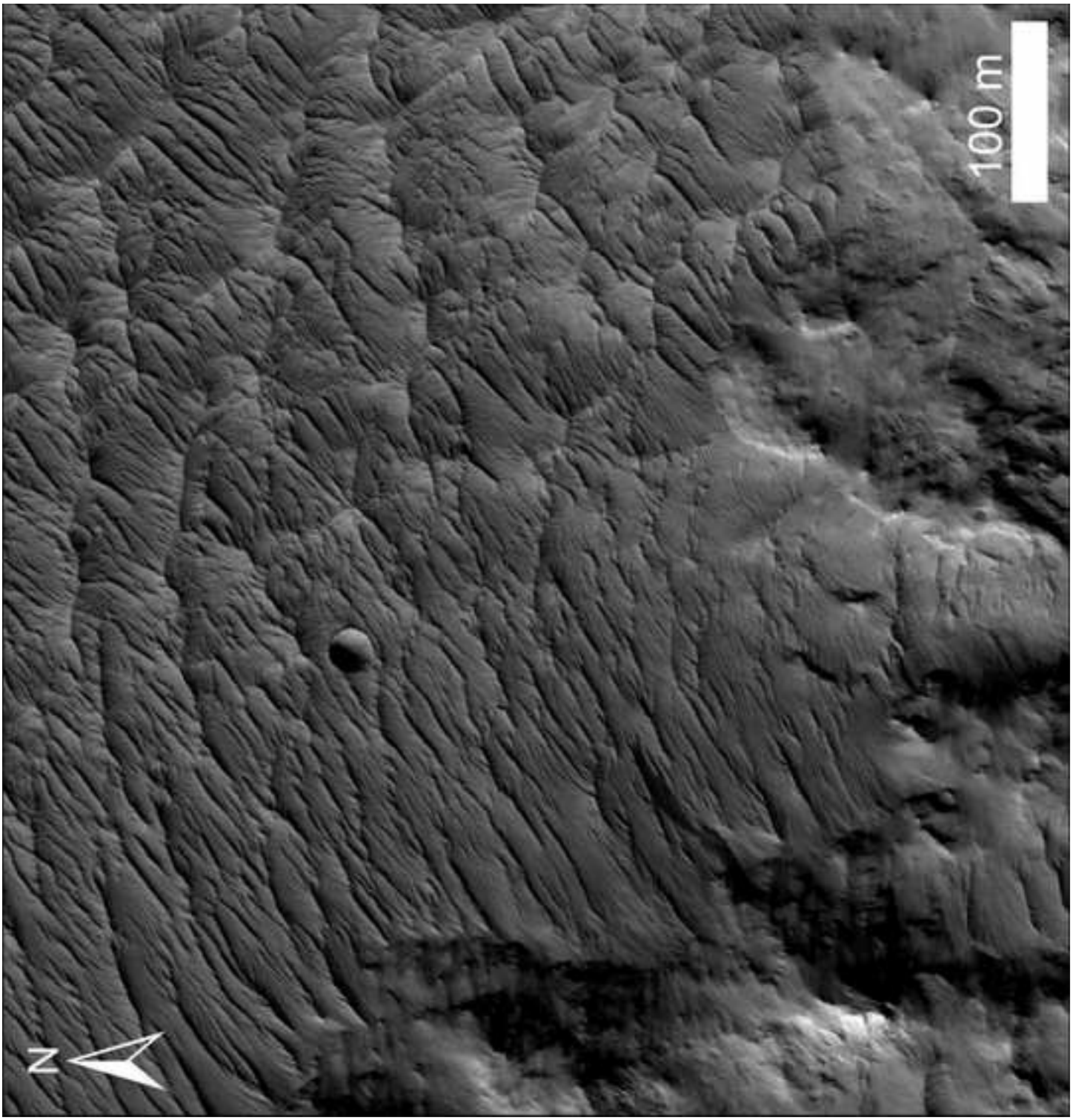

Figure

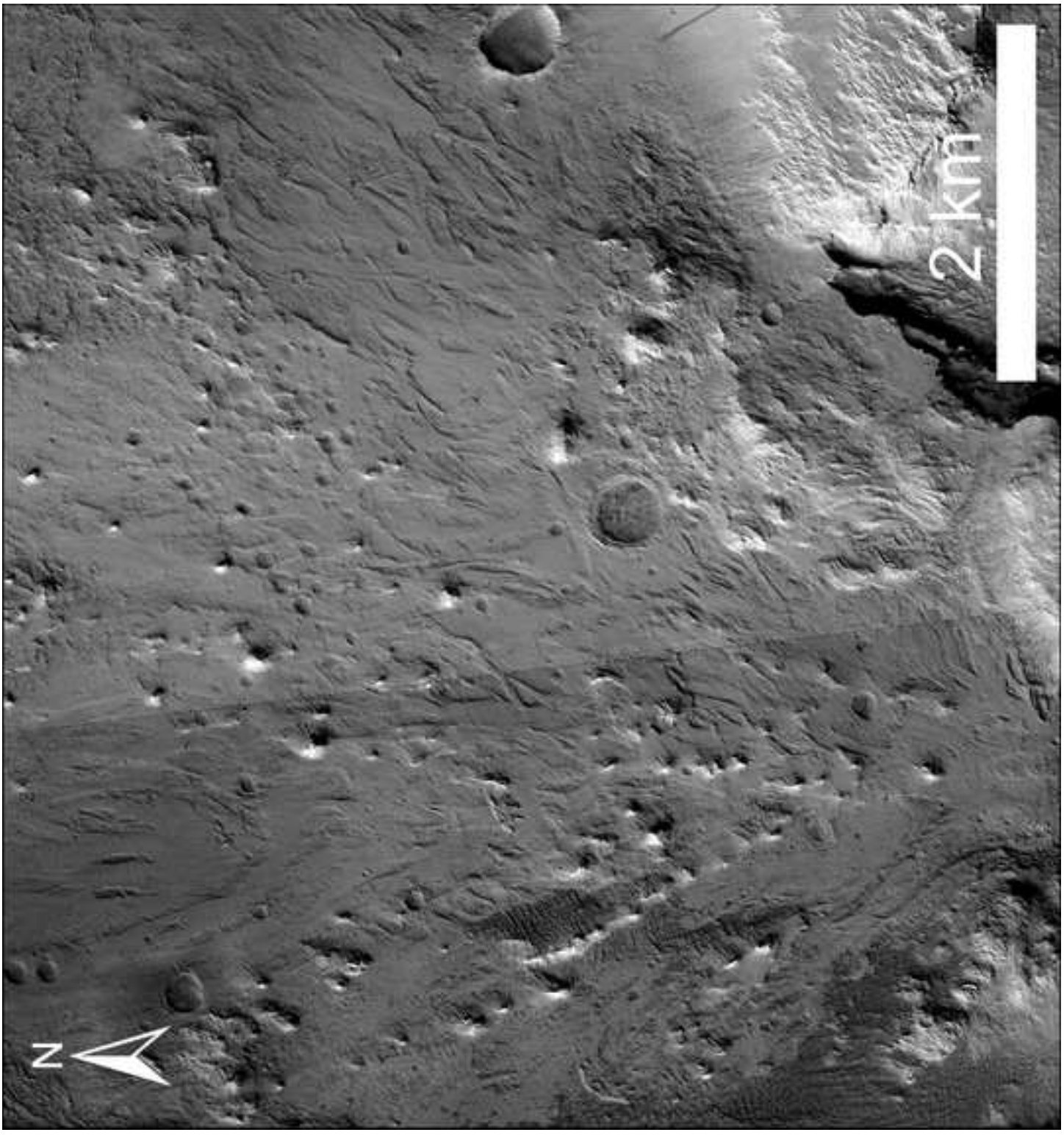

Figure

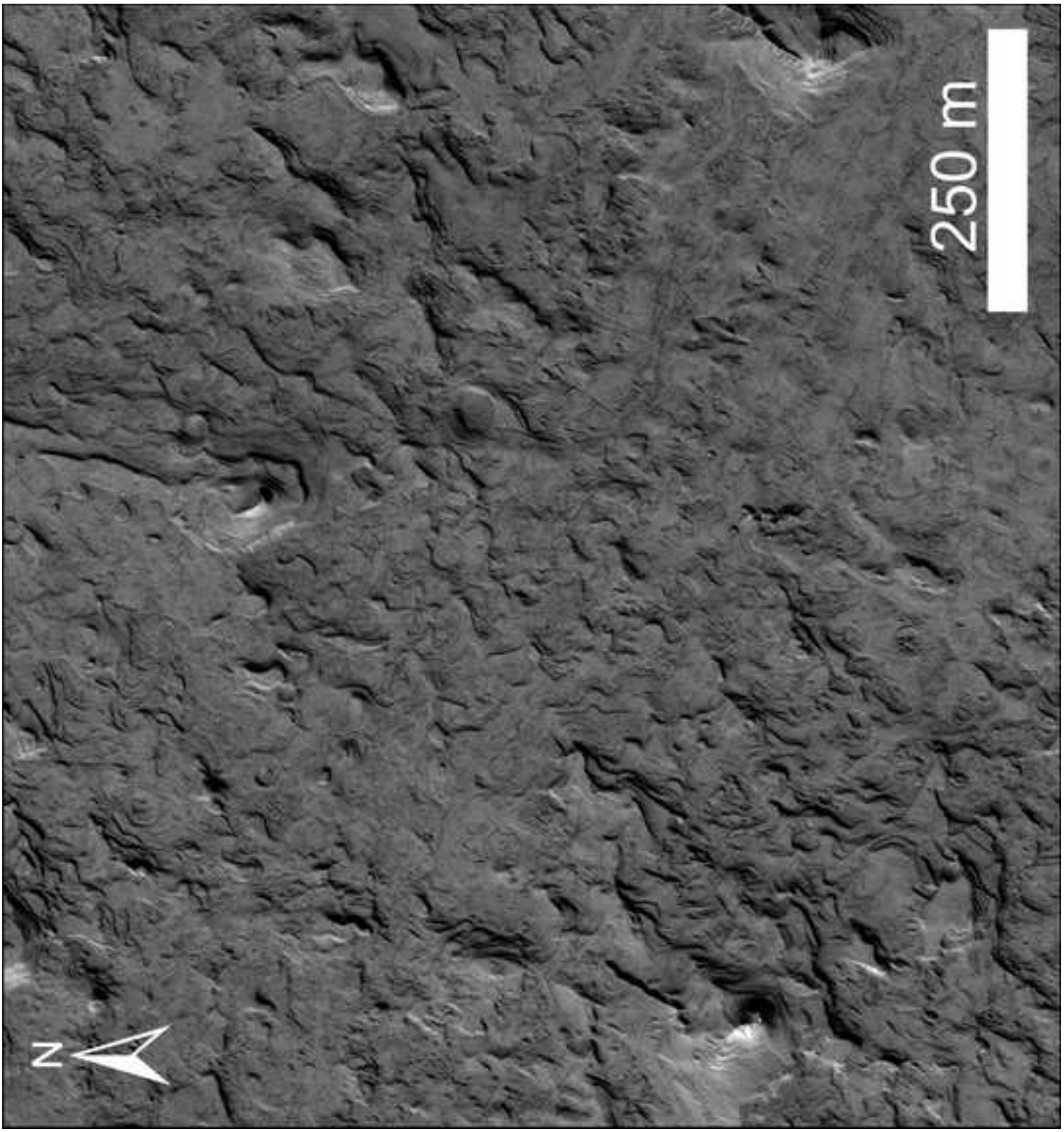

Figure

Figure

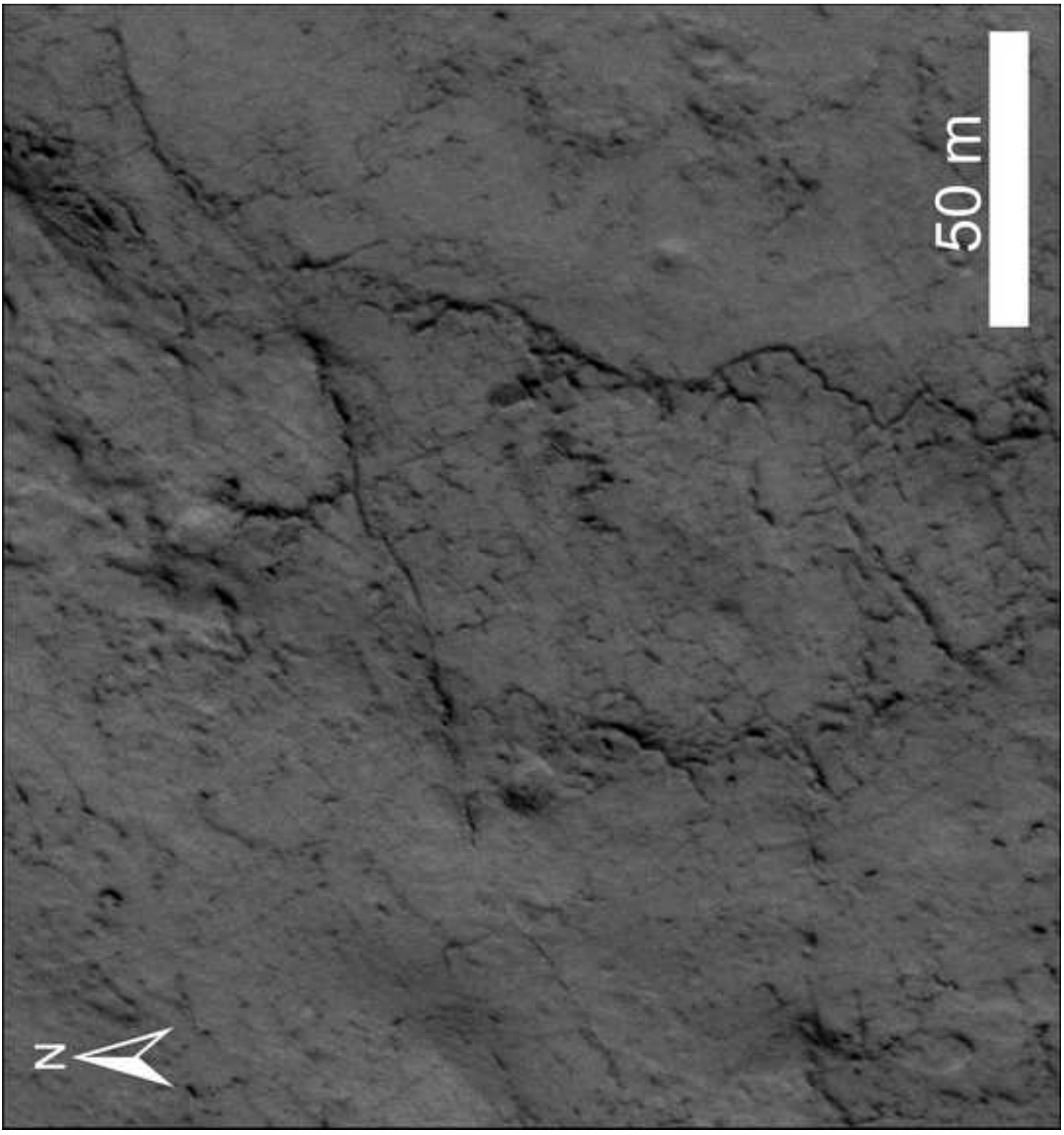

Figure

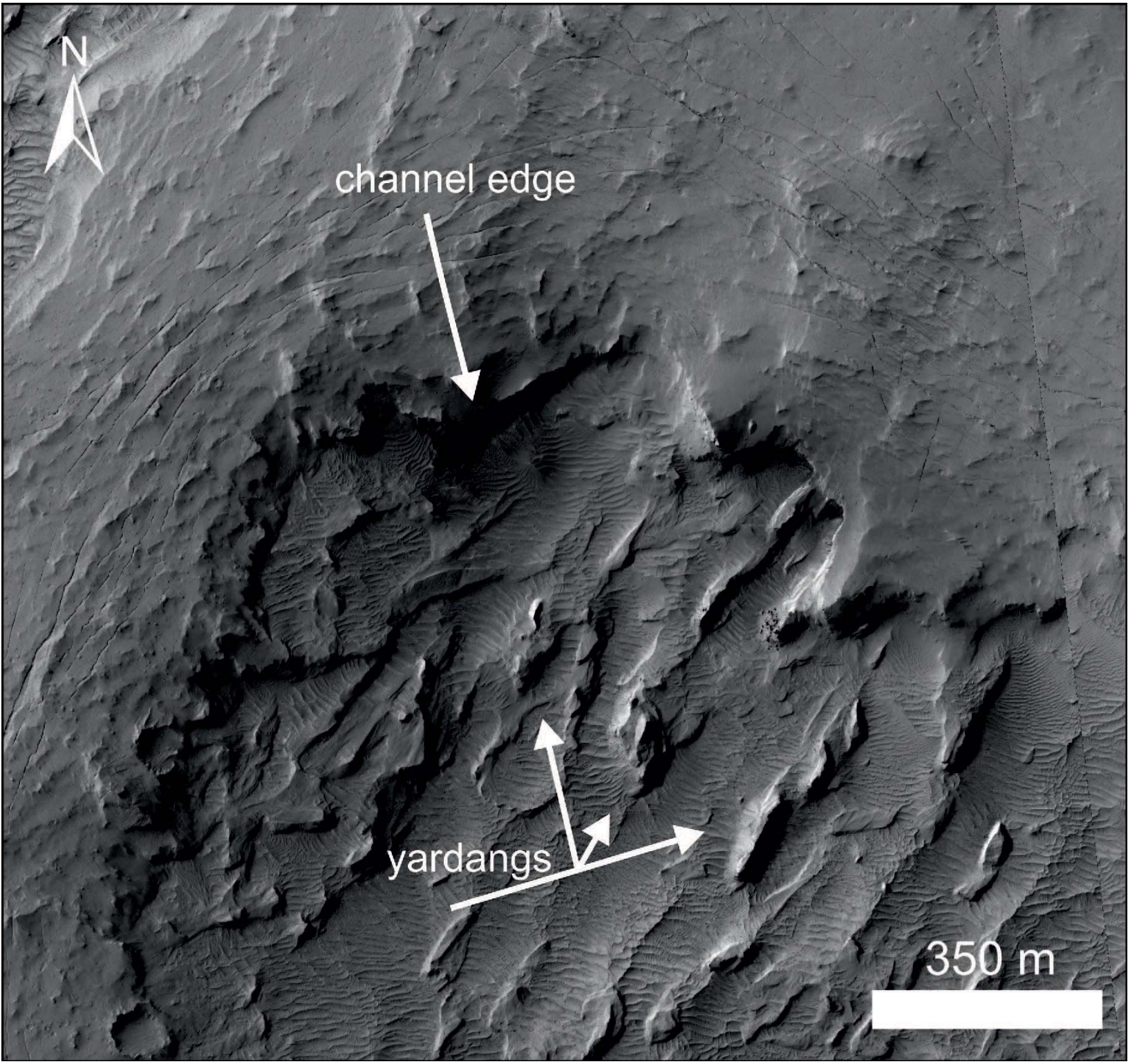

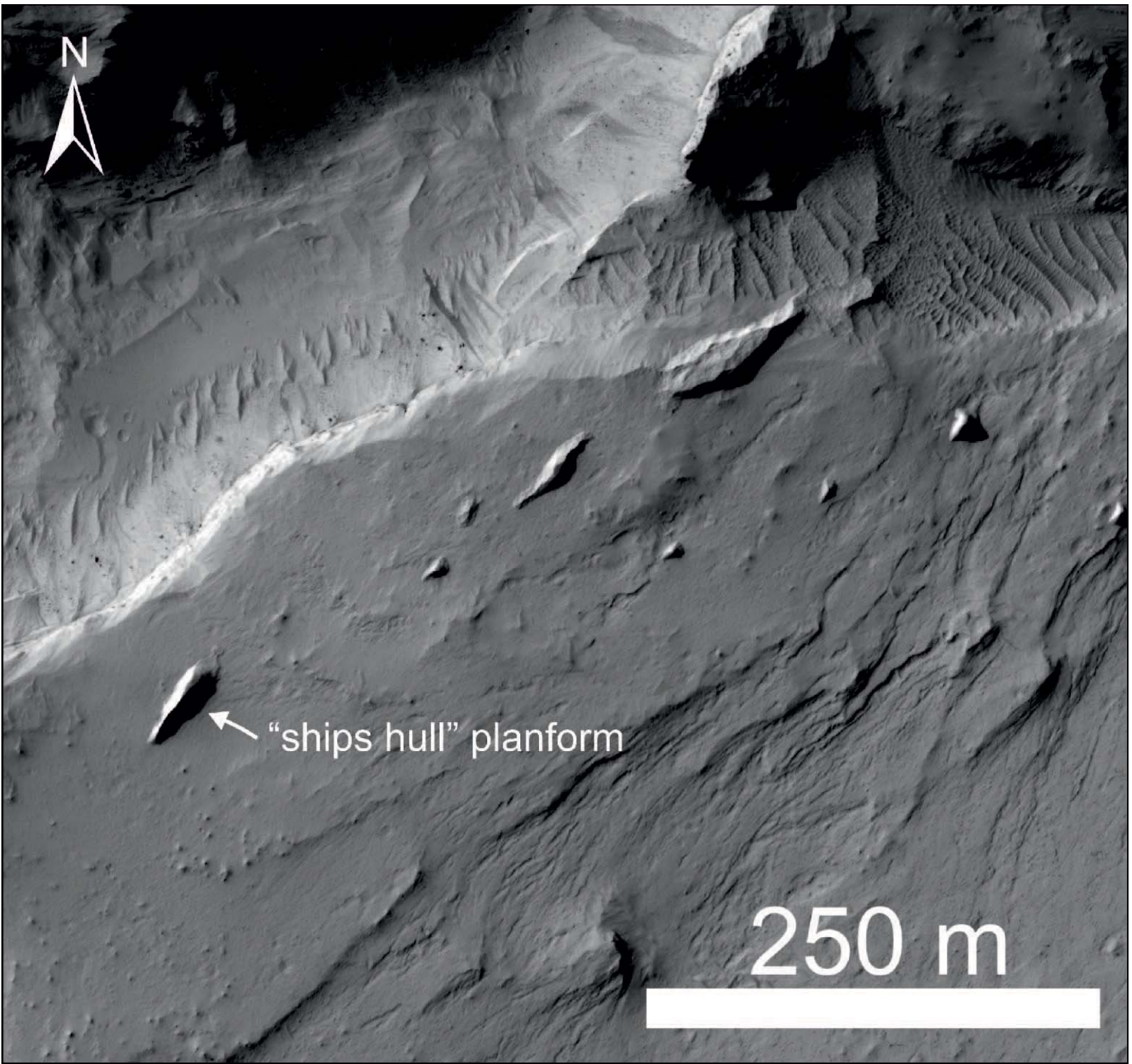

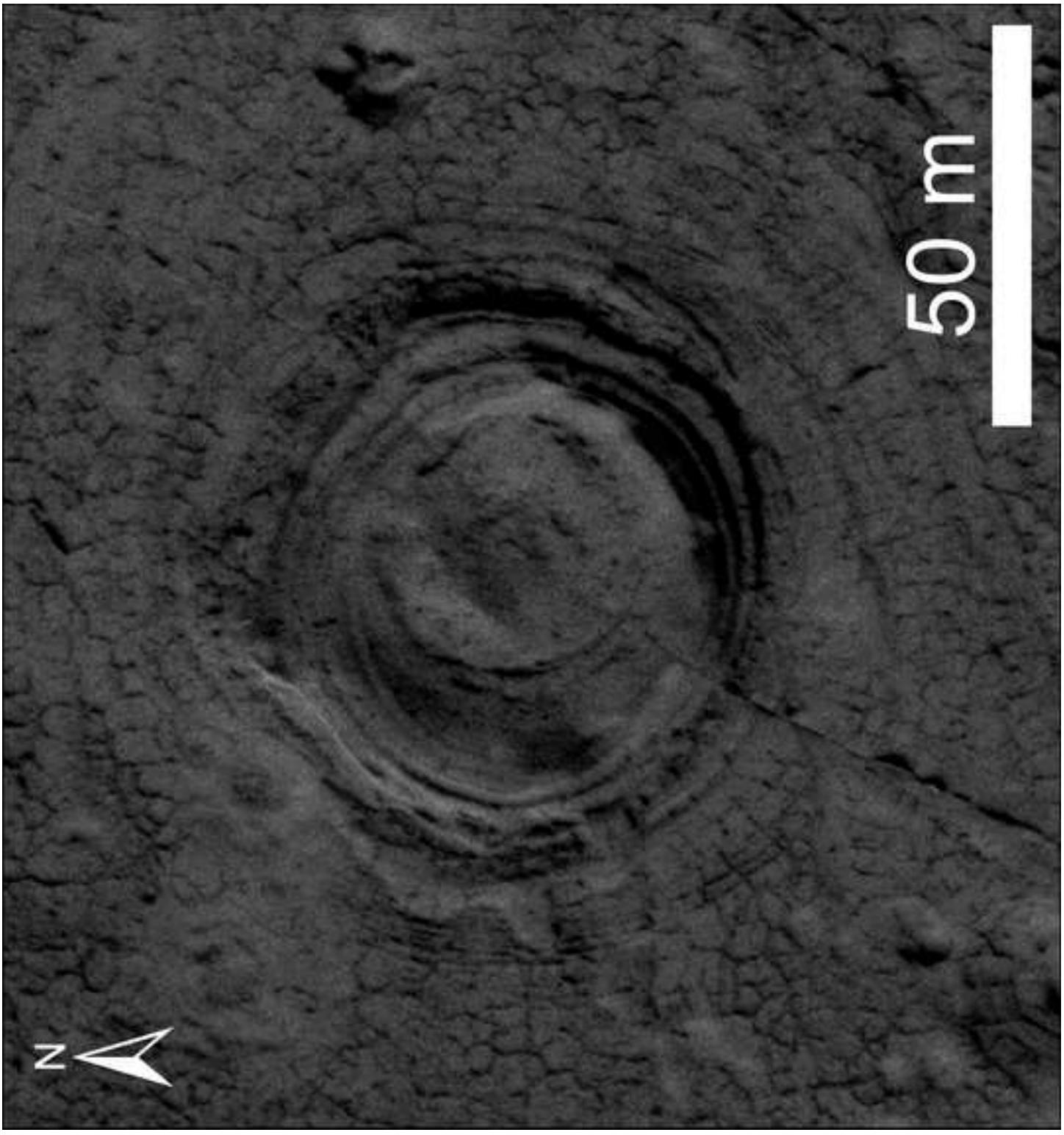

Figure

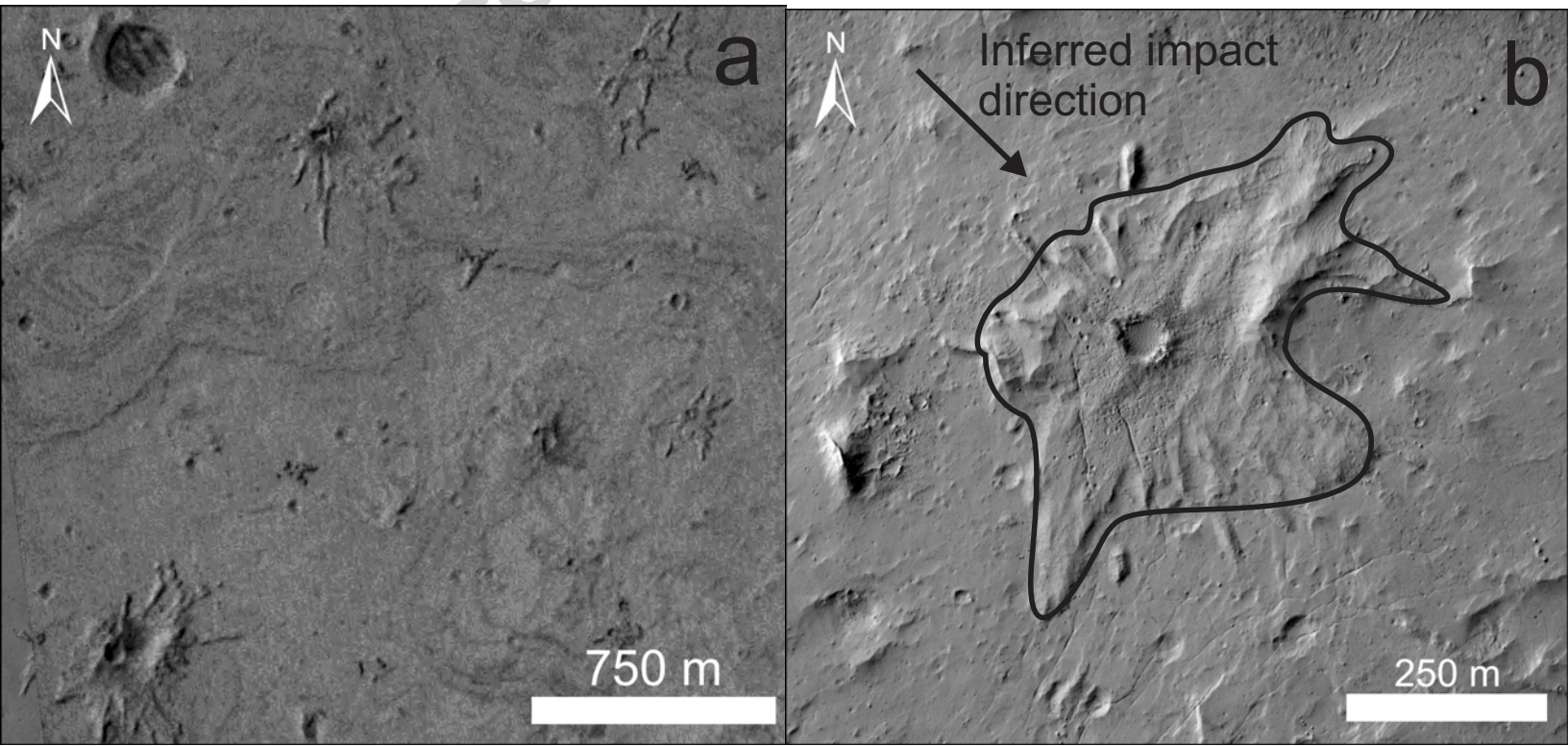

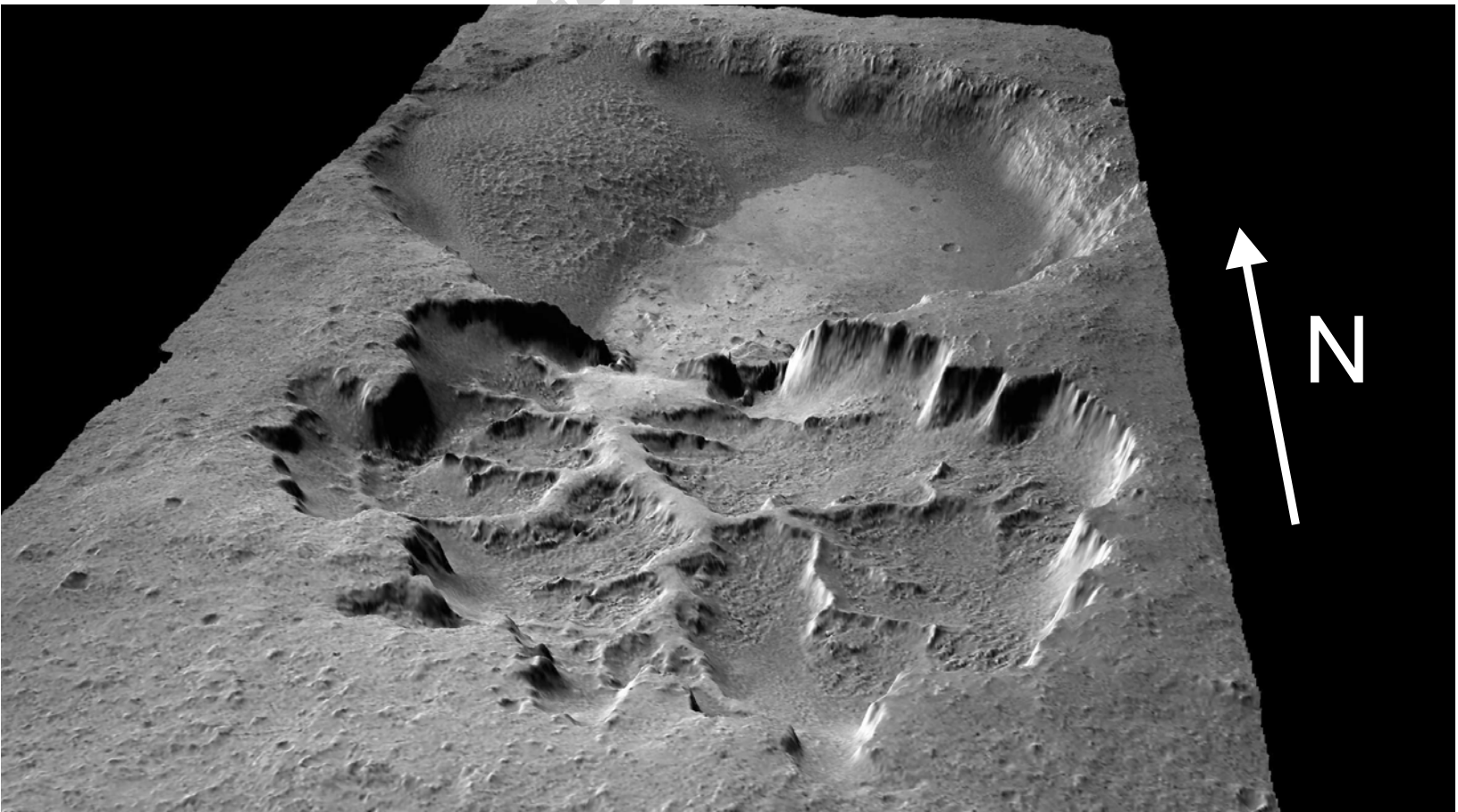

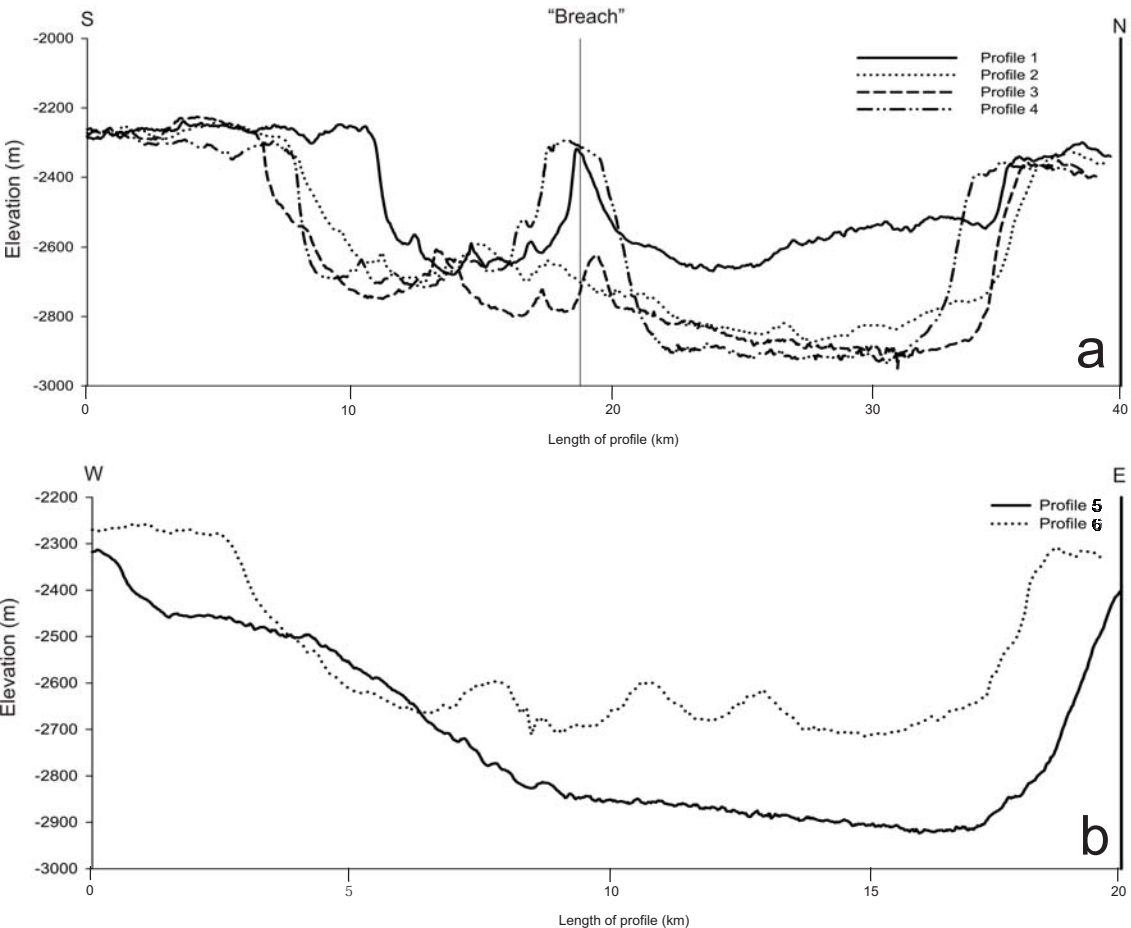

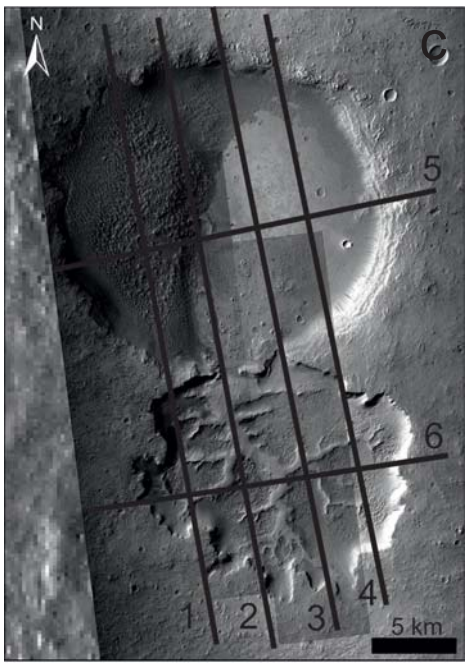

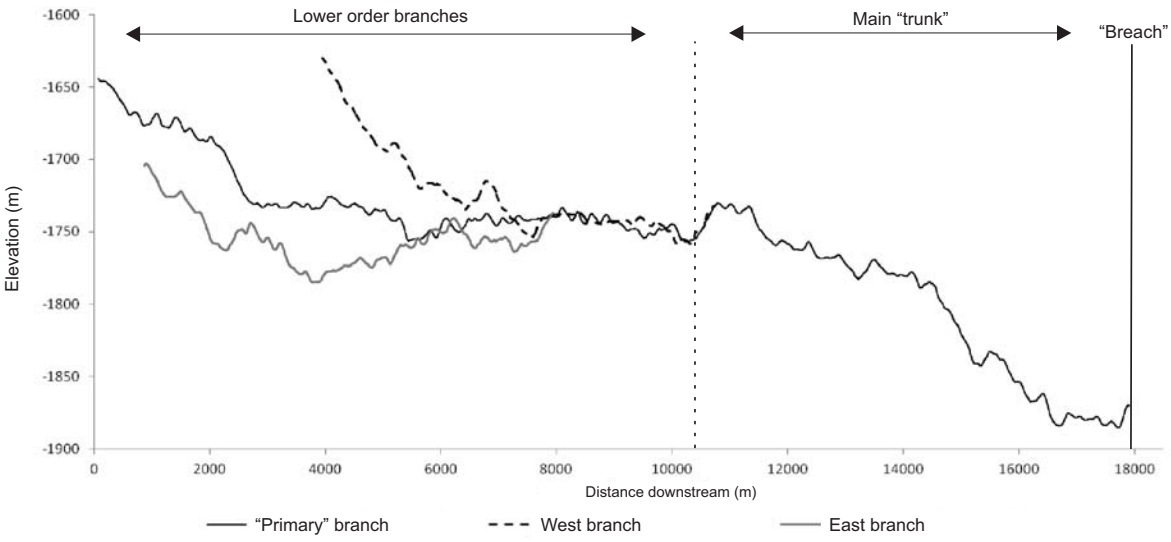

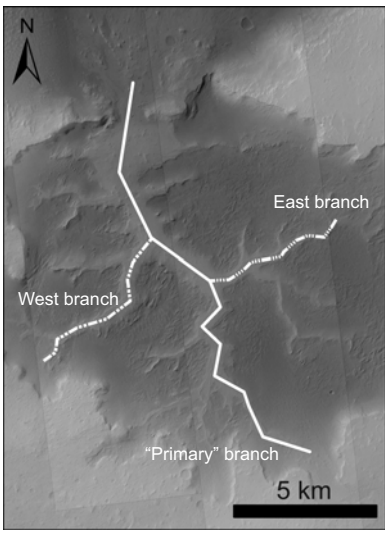

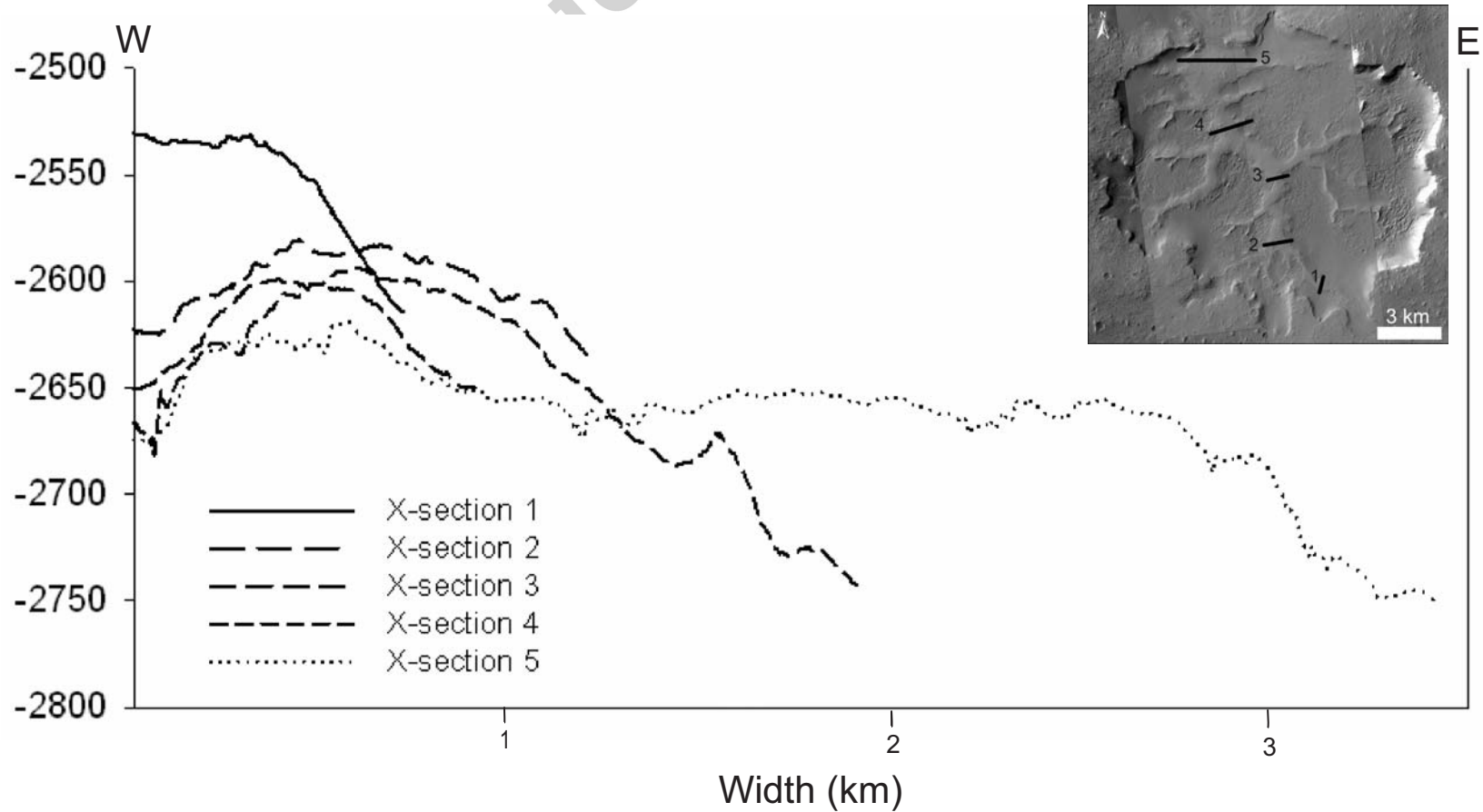

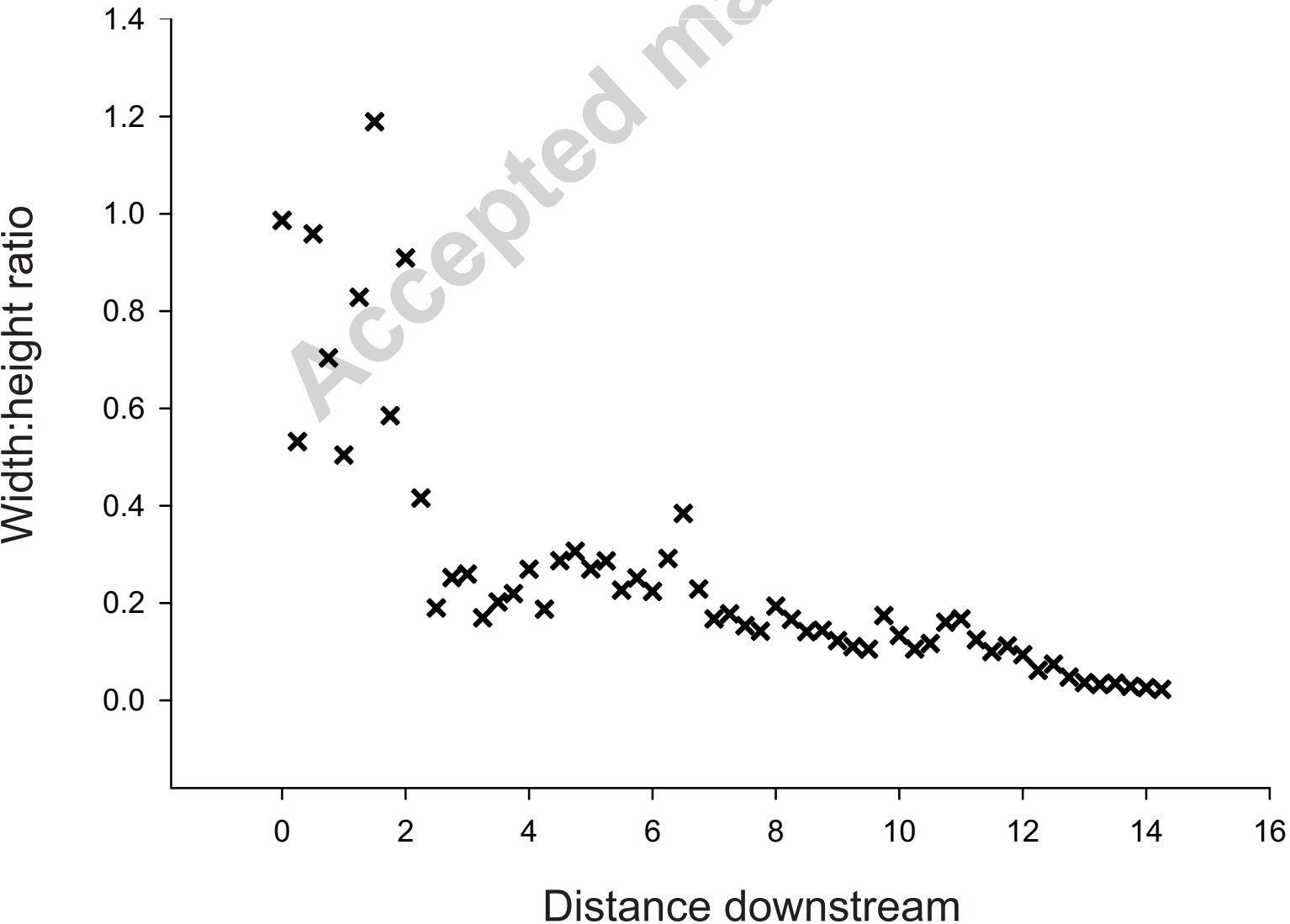

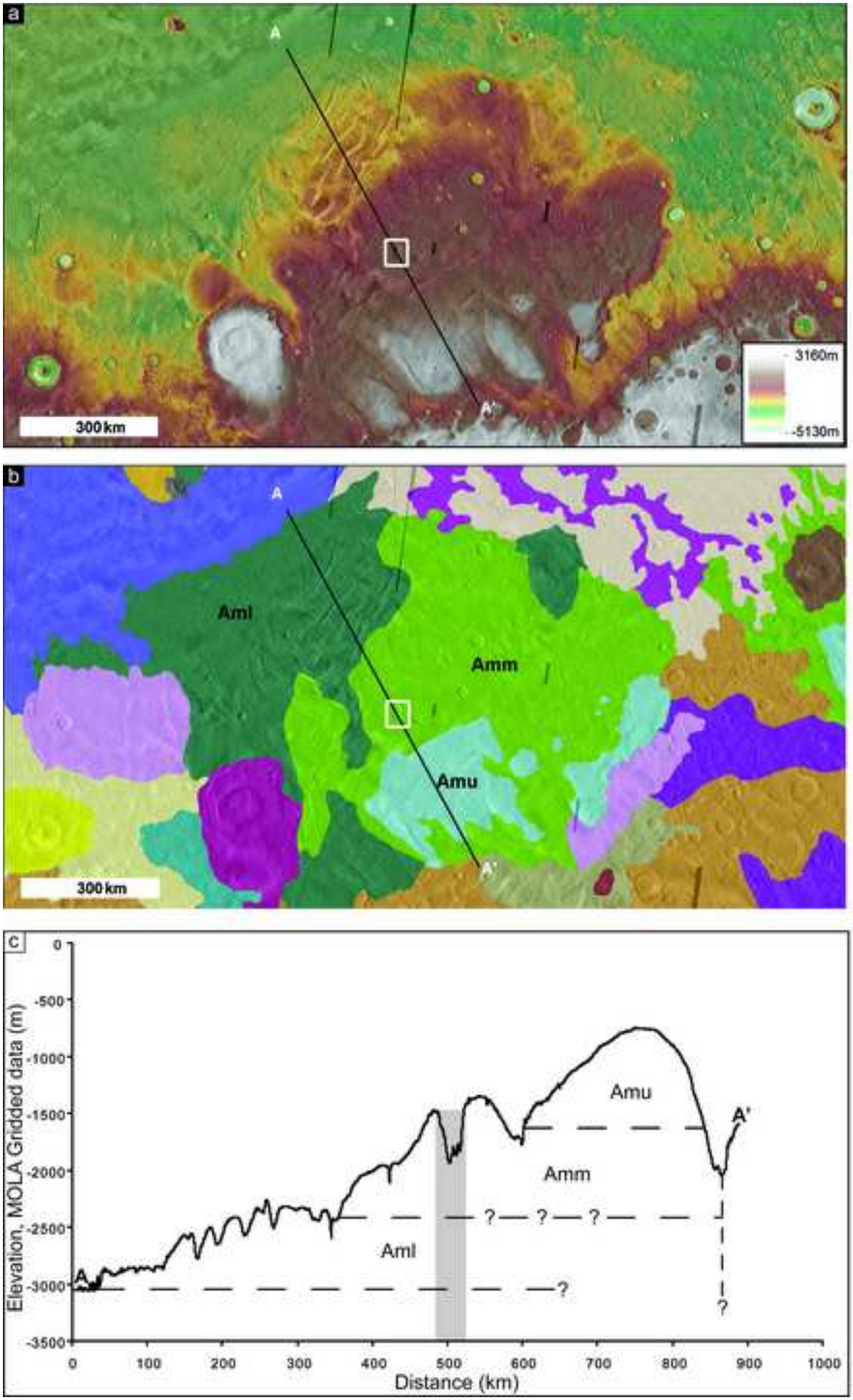

Figure

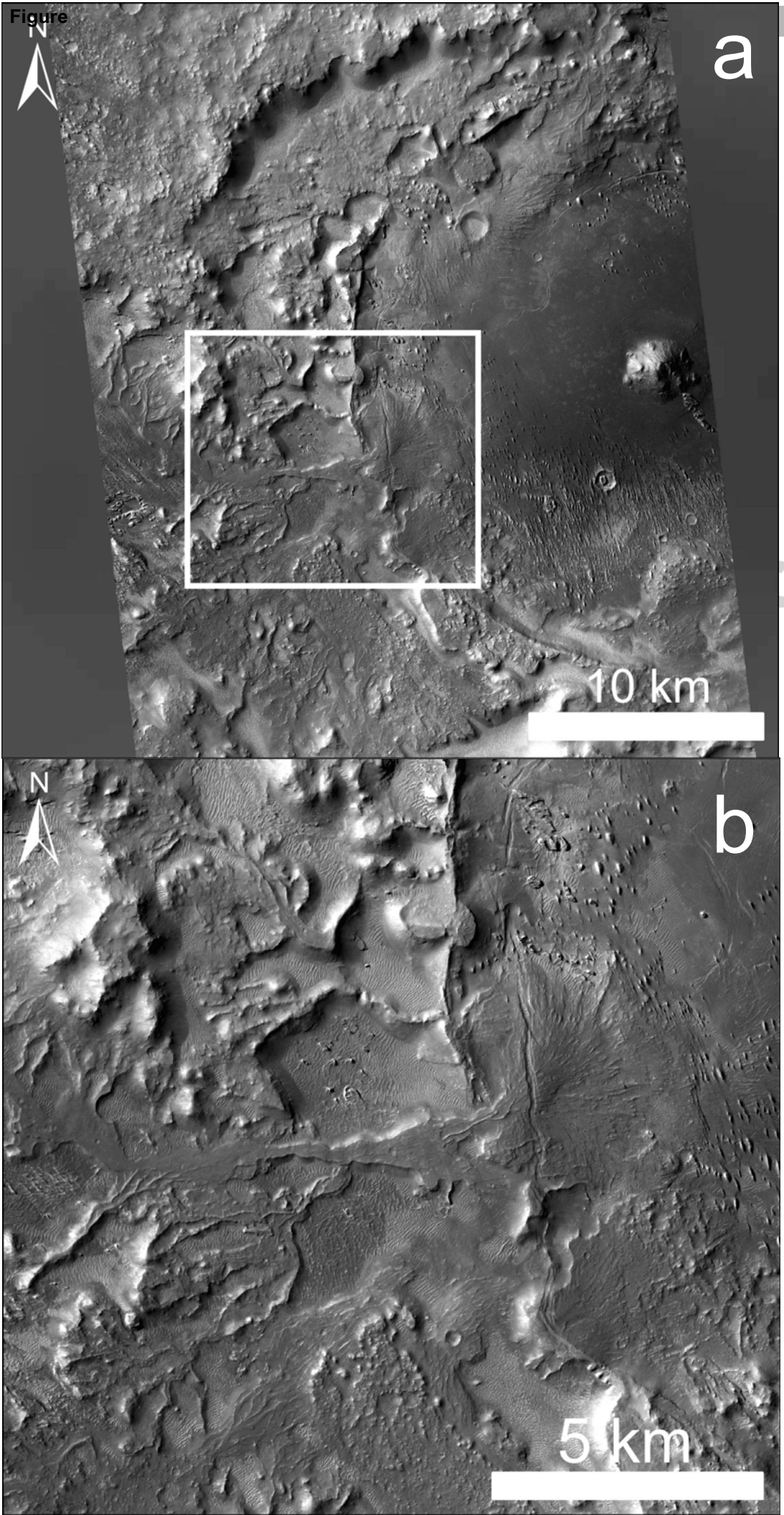

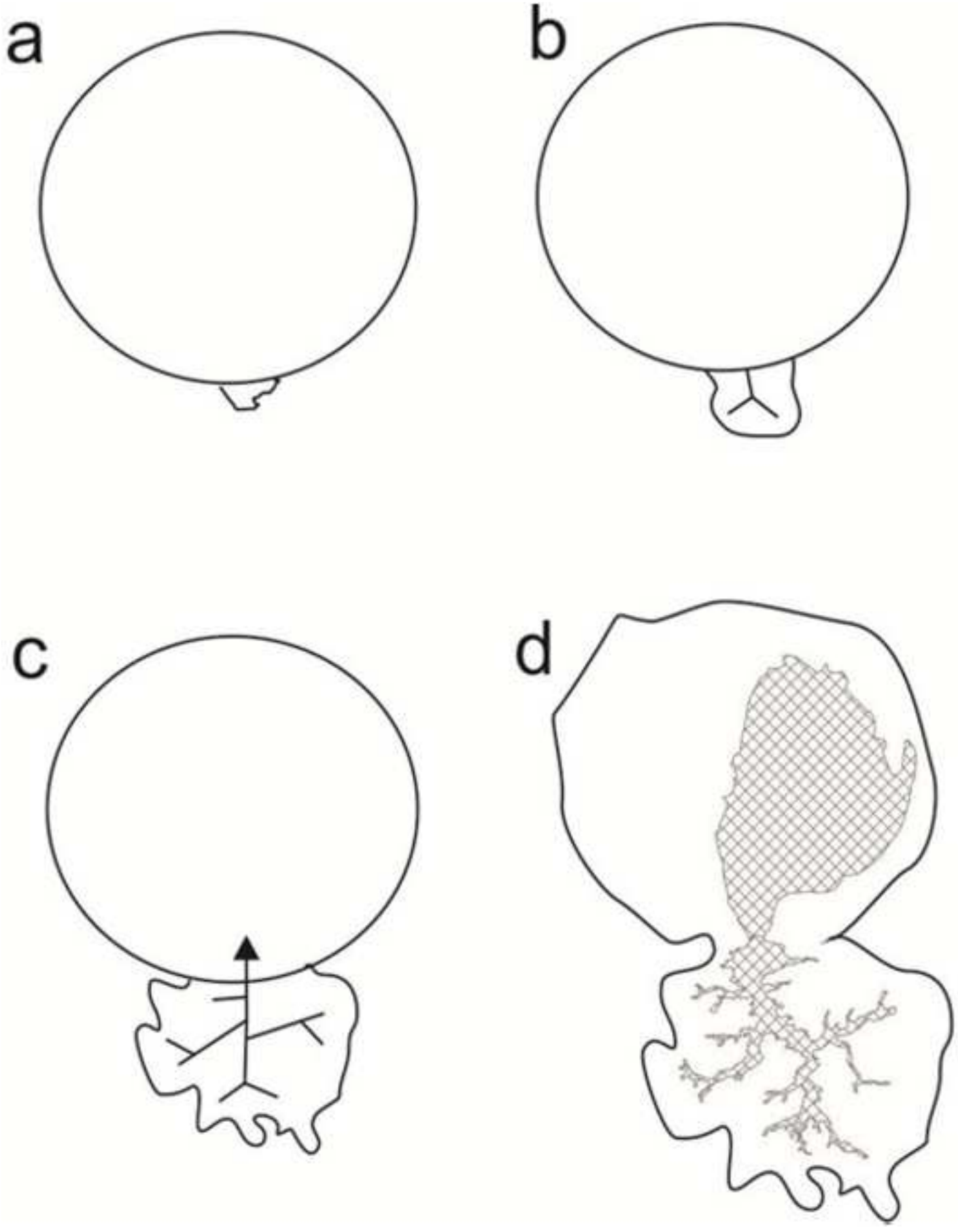

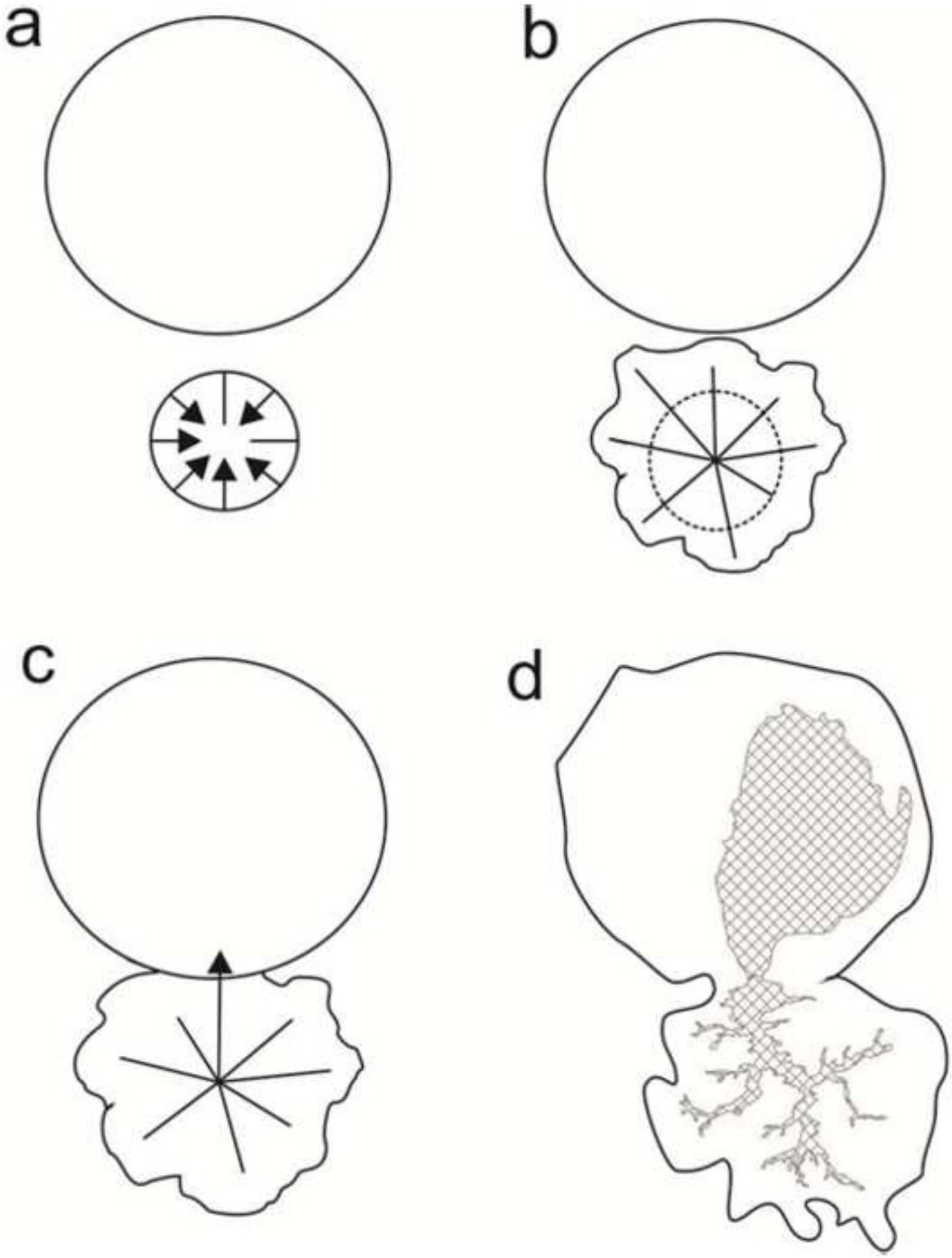

Tables

a

Cross-sectional shape	Width	Occurrence
Thin	on order of 10^1 m	34% (most common)
Rounded	10^1 m – 10^3 m	~ 5% (rarest)
Flat	> 10^3 m	30%
Multilevel	any stacked combination	18%

b

Network pattern	Definition	Occurrence
Isolated	Single SR not connected or closely adjacent to other SRs in field of view	Not given
Subparallel	Individual SRs roughly parallel to each other	27%
Branched	Individual SRs intersecting at angles of ~ 30-75°	41% (most common)
Random	SRs intersecting at > 75°	10% (rarest)

Table 1: Morphological classification scheme for SRs, after Burr et al., 2009. a – Cross-sectional classification, b – Network patterns.

a

Cross-sectional shape	Width	Height
Flat crested	on order of 10^1 m	< 1m to > 10 m
Narrow crested	< 10 m	< 10 m
Round crested	not given	~ 5 m
Multilevel	mostly flat crested, so 10^1 m	-

b

Network pattern	Definition
Branching	Interconnected SRs, either fan-like or braided
Non-branching	SRs isolated along length

Table 2: Morphological classification scheme for SRs, after Zimbelman and Griffin, 2010. a – Cross-sectional classification, b – Network patterns.